学位論文

Structural and functional analysis of the periplasmic region of B subunit in the sodium-driven flagellar stator

（ナトリウム駆動型べん毛モーター固定子Bサブユニットのペリプラズム領域に関する構造機能解析）

名古屋大学　大学院理学研究科　生命理学専攻

朱 世伟

ZHU Shiwei

Abstract

Bacterial flagellar motor is a miraculous rotary molecular machine and propels bacteria to swim toward favorable environment. The torque for flagellar rotation is generated by the rotor-stator interaction coupled with the ion (H^+ or Na^+) flow passing through the channel in the stator. The stator is dynamically assembled around the rotor and is believed to activate ion translocation activity only when it is with proper orientation around the rotor. The major problem is how the stator gets activated, especially for the Na^+-driven type.

This thesis investigates the stator activation using a chimeric Na^+-driven and a native Na^+-driven motor, respectively. A hybrid stator complex that is composed of a *Vibrio* PomA subunit and a chimeric B subunit (PotB) consisted of an N-terminal region of *Vibrio* PomB and a C-terminal region of *E. coli* MotB, has been convinced to work as the sodium-driven type in *E. coli* whose original motor is driven by proton motive force. In particular, we constructed a deletion variant of PotB (with a deletion of residues 41 to 91 [Δ 41-91], called PotB Δ L), which lacks the periplasmic linker region including the segment that works as a "plug" to inhibit premature ion influx. This variant did not confer motile ability, but we isolated a sodium-driven, spontaneous suppressor mutant, which has a point mutation (R109P) in the MotB/PomB-specific α-helix that connects the transmembrane and peptidoglycan binding domains of PotBΔL in the region of MotB. Overproduction of the PomA/PotBΔL(R109P) stator inhibited the growth of *E. coli* cells, suggesting that this stator has the high sodium-conducting activity. Mutational analyses of Arg109 and nearby residues suggest that the structural

alteration in this α-helix optimizes PotBΔL conformation and restores the proper arrangement of transmembrane helices to form a functional channel pore. It is speculated that this α-helix plays a key role in assembly-coupled stator activation.

The stator unit of the native Na^+-driven flagellar motor in *Vibrio* is composed of PomA and PomB, however, is thought to be fixed to not only the peptidoglycan layer but also the T-ring by the C-terminal periplasmic region of PomB. To compare *E. coli* MotB, we determined the crystal structure of a C-terminal fragment of PomB ($PomB_C$) at 2.0 Å resolution, and the structural information suggests a conformational change in the N-terminal region of $PomB_C$ for anchoring the stator. On the basis of the structure, we designed double Cys-replaced mutants of PomB for *in vivo* disulfide crosslinking experiments and examined their motility. The motility can be inhibited reversibly by reducing reagent. The results of these experiments revealed that the N-terminal two thirds of α1 (154-164) changes its conformation to form a functional stator around the rotor. The crosslinking did not affect the localization of the stator nor the ion conductivity, suggesting that the conformational change between the α1 helix and core domain of $PomB_C$ occurs in the final step of the stator assembly around the rotor.

In this study, it clearly demonstrates that the structural change of the C terminal α1 helix and core domain of the B subunit is important for the activation of stator function as well as for anchoring the stator unit. Dynamic structural change probably induces the channel opening of stator and subsequently the ion influx through the stator complex. However, it is still mysterious how the stator is associated and disassociated with the rotor.

Acknowledgment

I want to thank my thesis advisor, Michio Homma for the scientific guidance. He has been supportive of everything I did and is willing to listen and to help me solve my problem in a good way. His passion and enthusiasm always encourage me to study hard. I also would like to thank all the past and current members in the lab of Homma for your kindness in both my research and daily life. In particular, I want to give my appreciation to knowledgeable and critical Seiji Kojima who taught me everything he knows as an advisor, who gave me encouragement when I was frustrated, whom I could turn to talk about everything as a friend. I have to thank Na Li for teaching me some basic skills in the genetics when I just came here. Special appreciation has to go to Takehiko Nishigaki for all the interesting conversations. I also want to give my appreciation to Yasuhiro Onoue, Satoshi Inaba and Takashi Tsukamoto for their kind helps. I want to thank all graduate students. Especially I would like thank Mizuki Gouhara and Norihiro Takekawa for giving me some advice about my experiment, and Ananthanarayanan Kumar for wonderful discussion in both research and daily life. I also have to thank Eiko Hattori and Noriko Nishioka for assistance on many aspects of daily matters.

I deeply appreciate professor Katsumi Imada in Osaka University for giving me great encouragement and advice during my PhD study. I also thank Dr. Mayuko Sakuma who gave me many favors in the research and daily life. I want to thank Dr. Masayoshi Nishiyama for giving me great advice.

Finally, I express my sincere gratitude to my family. Due to their selfless love and financial support, I could dedicate myself entirely towards the PhD study. I often reproached myself and felt guilty for not being with them since I came to study here. However, they always encouraged me, tried to let me not worry about their health and focus on my research. I felt an eternal gratitude to them for what they have done for me. I also want to give my heartfelt thanks to my wife Li Zhang. Without your encouragement, trust and helps, I would not have been able to finish my dissertation. I could not express how grateful I am. You look like a beacon and bring me calmness and sunshine when I am in gloomy mood.

List of Abbreviation

DTT: Dithiothreitol

EDTA: Ethylenediaminetetraacetic acid

IM: Inner membrane

Laf: Lateral flagella

OM: Outer membrane

Omp-A: Outer membrane protein A

PEM: Periplasmic region essential for motiltiy

PG: Peptidoglycan

PGB: Peptidoglycan binding

PVDF: Polyvinylidene difluoride

SDS: Sodium dodecyl sulfate

SDS-PAGE: Sodium dodecyl sulfate-Polyacrylamide gel electrophoresis

NAM: N-acetylmuramic acid

Table of contents

Chapter 1:

General Introduction

Vibrio species are Gram-negative, rod-shaped bacteria that live in all types of aqueous environments including marine, freshwater and estuary (Blake *et al.*, 1980; Johnson *et al.*, 2012). All *Vibrio* species can move using flagella, which are cell surface organelles call flagella that propel them. *V. cholerae* has a single polar flagellum (monotrichous); whereas other species of *Vibrios* such as *V. parahaemolyticus* and *V. alginolyticus*, when exposed to viscous environments, produce enormous numbers of flagella at lateral or peritrichous positions (called "lateral flagella") in addition to the single polar flagellum (Fig. 1A) (McCarter *et al.*, 1988; Kawagishi *et al.*, 1996). Each polar flagellum is covered with a sheath that is contiguous with the outer membrane, making it thick and hence can be observed using dark-field microscopy with a mercury lamp. Lateral flagella are not covered with a sheath, so they are difficult to observe using light microscopy. In *V. alginolyticus*, the polar flagellum is responsible for the swimming in liquid environment, whereas the lateral flagella are responsible for the swarming in non-liquid environment (McCarter, 2004). Although the polar and the lateral flagella are distinct from each other in the function, the basic structures of the flagellum in *Vibrio* species are the same to those in other species (Fig. 1) (Aizawa, 1996; Chen *et al.*, 2011). Unlike eukaryotic flagella, the flagellar rotation in bacteria is dependent on the ion-motive force across the cell membrane (Berg, 2003; Terashima *et al.*, 2008). A functional flagellum basically consists of a filament acting as a helical propeller, a hook functioning as a universal joint and a basal body working as a rotary motor (Fig. 1) (Sowa and Berry, 2008; Li *et al.*, 2011).

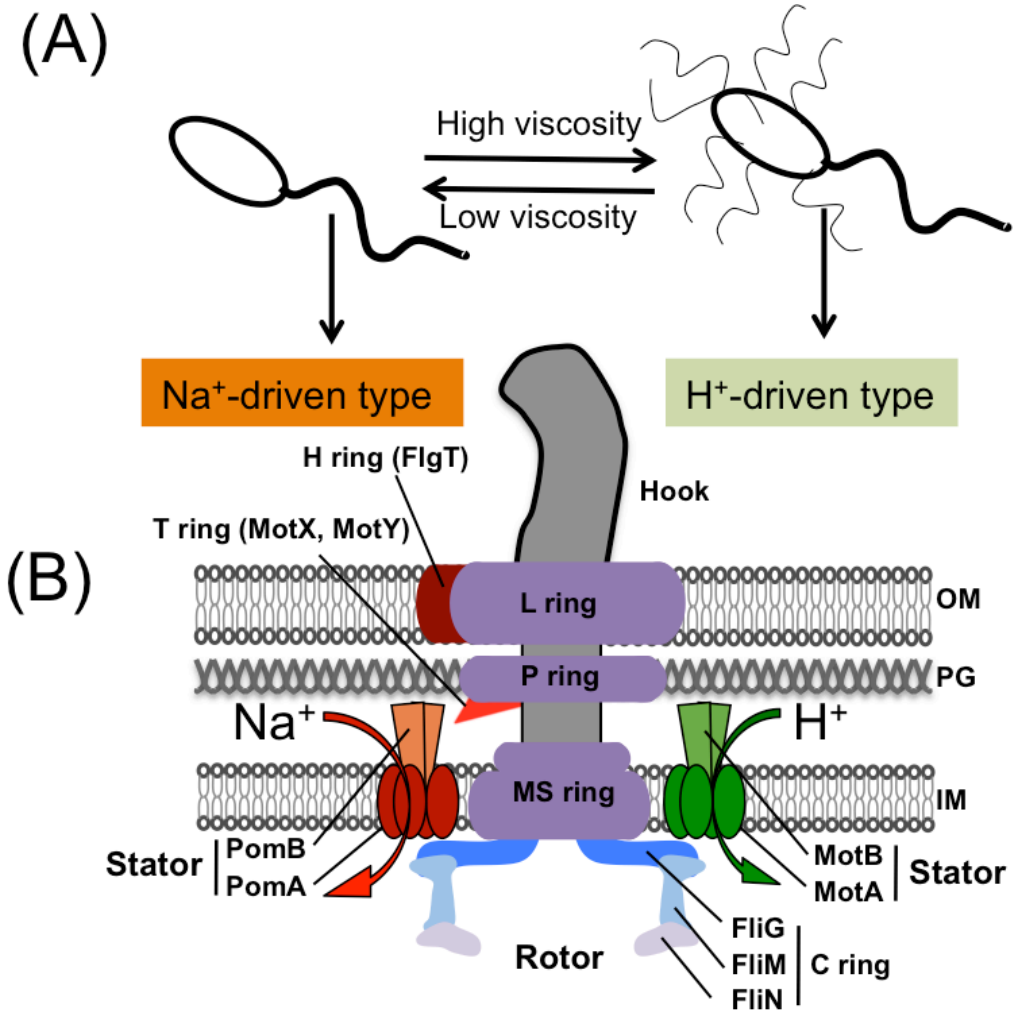

Fig. 1. Flagellar structure of *Vibrio*.

(A) Polar flagellum and lateral flagella in *Vibrio* species excluding *Vibrio cholerae*. (B) Schematic diagram of the hook basal body for a polar flagellum shown in the left half (based on EM images, (Terashima *et al.*, 2006; Terashima *et al.*, 2013) and the lateral flagellar structure shown in the right half is based on the peritrichous flagellum from *Salmonella*) (Macnab, 2003). The characteristics of the polar flagellum are the H ring and the T ring, shown by arrows in the left half.

The overall structure of the flagellar basal body is shown schematically in Fig. 1B, based on electron microscopic images of the purified hook-basal body from a peritrichous flagellum of *Salmonella enterica* (right side) and from a polar flagellum of *Vibrio alginolyticus* (left side) (Francis *et al.*, 1994; Thomas *et al.*, 2006; Terashima *et al.*, 2008; Terashima *et al.*, 2013). Both kinds of basal bodies share common features even though they originate from different species of Gram-negative bacteria: the hook and basal body with several rings embedded in the cell envelope (Fig 1). The flagellar basal body functions as a rotary motor and consists of two parts: the rotary part (rotor) and the stationary part (stator). The rotor contains several rings: from the cytoplasmic face, there is the C ring (also called the "switch complex") composed of FliG, FliM and FliN and the MS ring embedded in the cytoplasmic membrane (made of at most 26 copies of FliF). These rings are connected by a rod whose tip connects to the hook. The basal body contains two other rings, the P ring (FlgI), which is associated with the peptidoglycan layer and the L ring (FlgH), which is located in the outer membrane (Aizawa, 1996; Terashima *et al.*, 2008). Thus the LP ring does not rotate but functions as a bushing for the central rod.

The polar flagellum of *Vibrio* contains two additional ring structures, named the T ring which surrounds the periplasmic side of the P ring (Terashima *et al.*, 2006) and the H ring which is located at the outer rim of the L ring. The T ring is made of two proteins namely MotX and MotY. They are essential components of the polar flagellar motor of *Vibrio* and are probably involved in stabilizing the stator surrounding the rotor (McCarter, 1994a; b; Okabe *et al.*, 2001; Terashima *et al.*, 2006). The crystal structure

of MotY from *V. alginolyticus* in conjunction with biochemical analysis revealed that the C-terminal domain of MotY stabilizes the association with the peptidoglycan layer and that the N-terminal domain of MotY is involved in the association with the basal body (Kojima *et al.*, 2008b). The H ring is located at the outer rim of the LP ring, so we initially thought that the LP ring was somehow bigger in this basal body (Fig. 1 and Fig. 2). The loss of *flgT* results in an almost non-motile phenotype and there is no formation of the T ring in addition to the lack of an outer rim structure of the LP ring. Therefore FlgT is likely to be a component of the H ring and is also important for assembly of the T ring. Our crystal structure and functional analyses of FlgT support this idea (Terashima *et al.*, 2013). Perhaps these two unique extra ring structures in the polar flagellum are required to fix the stator units around the rotor (Fig. 2). The polar flagella of *Vibrio* can rotate extraordinarily up to 1,700 Hz (Magariyama *et al.*, 1994), while the rotational speed of the H^+-driven flagellar motor is just around 300 Hz (Chen and Berg, 2000).

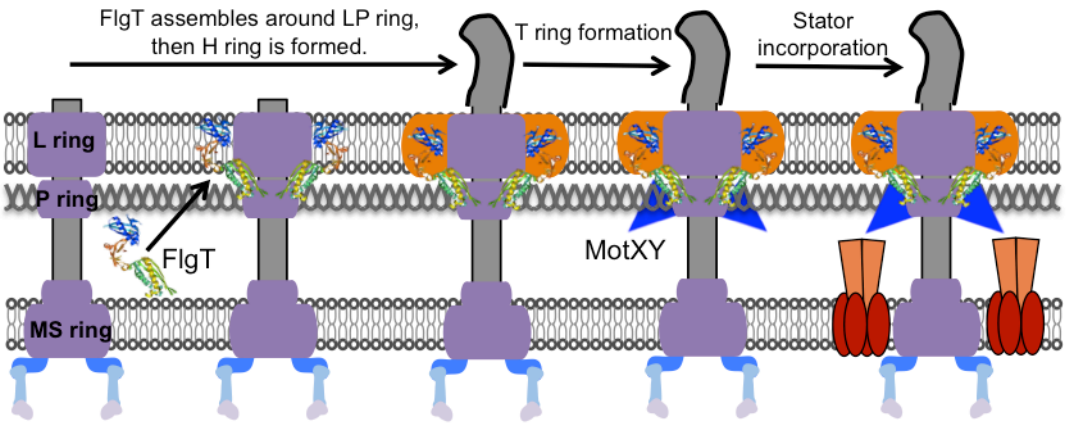

Fig. 2. Model for the basal body ring formation of the Na^+-driven polar flagellum.

The H ring construction is dependent on FlgT proteins that assemble around the previously formed L ring and P ring. Next, MotX and MotY assemble around the basal body to stably form the T ring with the help of the middle domain of FlgT. As a result, the stator is incorporated properly and works in the presence of the T ring. The model is drawn based on a previous report (Terashima *et al.*, 2013).

The energy source for flagellar rotation comes from the ion flux through the stator when it interacts with rotor. Although functional analysis suggests the possibility of an interaction between A subunit of stator and FliG (Zhou *et al.*, 1998a), intact images of the entire flagellar motor have remained ambiguous until recently due to the complexity of the stator units, which dynamically associate and disassociate from the rotor (Leake *et al.*, 2006; Murphy *et al.*, 2006). In 2006, Murphy and co-workers showed the first structure of the complete flagellar motor of the spirochete *Treponema primitia in situ* using the whole cell electron cryotomography method (Murphy *et al.*, 2006). Their images captured electron densities corresponding to the stator units surrounding around the rotor, revealing the relative locations of the C-ring and the stator units for the first time.

The stator of the H^+-driven motor of lateral flagella from *E. coli*, *Salmonella* and *Vibrio* is composed of two proteins, MotA/MotB (LafT/LafU for *Vibrio*), that of the Na^+-driven polar flagellar motor of *Vibrio* consists of PomA/PomB (Fig. 1). Both MotA and PomA contain 4 transmembrane segments (TM1 to TM4) and a large cytoplasmic loop between TM2 and TM3 (Fig. 3). Conserved charged residues in this loop are suggested to be responsible for the electrostatic interactions with some residues in the FliG (Zhou *et al.*, 1998a; Yakushi *et al.*, 2006). Both MotB and PomB have a single N-terminal transmembrane segment and a large C-terminal perplasmic region (De Mot and Vanderleyden, 1994; Asai *et al.*, 1997). This periplasmic region includes a peptidoglycan-binding motif (PG-binding motif) because it has a high structural similarity with Omp-A like protein which is well known for interacting with PG layers

(Koebnik, 1995). When the PG-binding motif is replaced with Pal protein, a kind of outer membrane protein in *E. coli*, the new hybrid stator does function (Hizukuri *et al.*, 2009), thus suggesting that the large periplasmic region of PomB will anchored to the PG layer around the rotor. Stator can act as a channel for ion flow only when it assembles around rotor. In the N-terminus of this periplasmic region, a short segment (residues, from 52-65 in *E. coli* but from 44-58 in *V. alginolyticus*) works as a plug to control the ion influx before the stator complex assembles around rotor (Hosking *et al.*, 2006; Morimoto *et al.*, 2010a; Li *et al.*, 2011). Since an overproduction of MotA/MotB does not affect growth inhibition (Stolz and Berg, 1991), but an overproduction of stator protein without the plug segment does due to massive ions flowing into the cells (Morimoto *et al.*, 2010a; Takekawa *et al.*, 2013). In addition, a conserved residue Asp in the TM segment of both MotB and PomB (Fig. 3) is recognized as the binding site of coupling ions (Zhou *et al.*, 1998b; Sudo *et al.*, 2009; Terashima *et al.*, 2010).

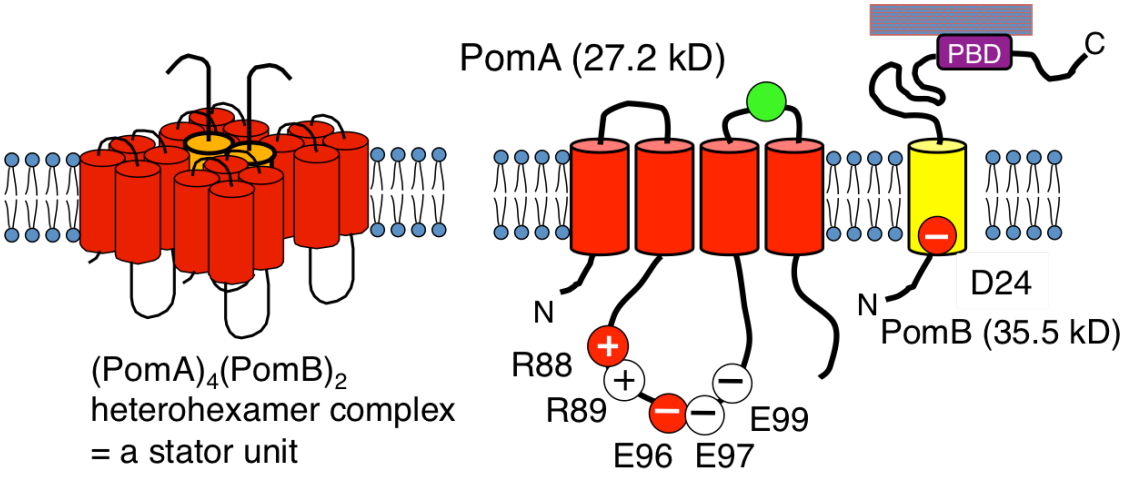

Fig. 3. The composition of the Na^+-driven stator. Functional stator unit is composed of 4 monomers of PomA and 2 monomers of PomB as shown in the left picture. PomA monomer contains 4 transmembrane segments TM1, TM2, TM3 and TM4 shown from left to right and a large cytoplasmic loop containing some important charged residues labeled in the red color. PomB monomer is composed of a single transmembrane segment where sodium binding site is labeled in the red color and a large periplasmic region containing periplasmic binding domain (PDB) labeled in the purple color.

Another important property of stator is its dynamic movement. In the *E. coli* H^+-driven motor, fluorescent photobleaching observation firstly indicates that the stator units are not really static components of the motor but can dynamically associate with and dissociate from the rotor (Leake *et al.*, 2006). Such a dynamic property can also be observed for the PomA/PomB stators of the *Vibrio* polar flagellum. Their assembly around the rotor is dependent on the external Na^+ concentration (Fukuoka *et al.*, 2009). Removal of sodium ions from the medium caused the dissociation of the stators from the rotor, and the subsequent addition of Na^+ to the medium restored the stator incorporation to the motor. The physiological meaning of the dynamic property of the stator is not known, but the rapid and stable rotation of the motor may be due to the stator dynamic property (Leake *et al.*, 2006).

The fact that dynamically assembled stator conducts ions only when it is so closed to the rotor, indicates that stator has at least two types: inactive and active respectively (Fig. 4). This raises a question: how is the ion conduction of the stator regulated? It is inferred that the mystery behind stator activation from the inactive to the active lies in the periplasmic region of PomB. The recently resolved crystal structure of the C-terminal periplasmic region of MotB from *Helicobacter pylori* and *Salmonella enterica* serovar Typhimurium shows an OmpA-like character (Roujeinikova, 2008; Kojima *et al.*, 2009), throwing some light on the structural information of stator in detail. Roujeinikova's group resolved the C-terminal structure of $MotB_C$ with N-acetylmuramic acid (NAM), which is basic component for forming the glycan chains. This shows that the stator is anchored in the peptidoglycan layer, however they did not

do any functional analysis of the stator (Roujeinikova, 2008). It is worth to note that a MotB mutant with the deletion of residues 51-110 and 271-309 is also functional, in spite of being unstable (Muramoto and Macnab, 1998), thus indicating that the essential periplasmic region for motor function is only the residues 111-270, henceforth referred to as PEM (Periplasmic region Essential for Motility). Kojima *et al.* resolved the *Salmonella* $MotB_C$ that just cover the PEM. A point mutation L119P or L119E at the long N-terminal α helix disrupts hydrophobic interaction between the helix and core domain of $MotB_C$ and results in high conductivity of ion and enhanced stator assembly (Kojima *et al.*, 2009). Thus they proposed a hypothesis about the activation of *Salmonella* proton-driven stator: when inactive stator is incorporated into the motor, a conformational change involved in the α helix and the core domain of $MotB_C$ might be trigged to activate stator function. However, owing to the lack of experimental evidence for the conformational change, the detailed molecular mechanism by which the stator couples the ion flow to flagellar rotation is still obscure. Whether the hypothesized conformational change in the H^+-driven stator still works in the Na^+-driven stator is yet to be investigated.

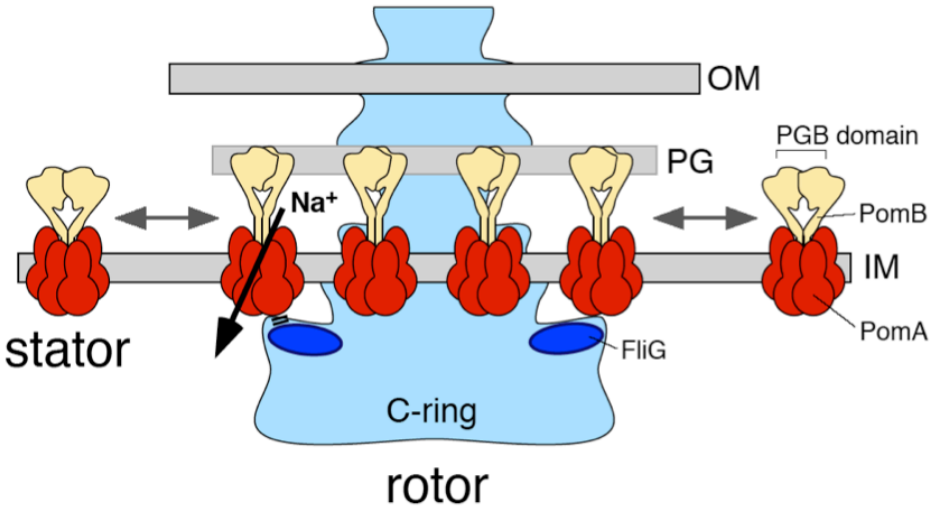

Fig. 4. Dynamic assembly of the Na^+-driven stator. The stator being far away from rotor represents inactive form. The stator so closed to the rotor represents the active form. In the active form, ion conductivity of stator will be triggered and finally transfer into mechanical energy for torque generation of flagellar rotation.

In this study, we investigated how the stator gets activated during the step of assembly around rotor. A chimeric Na^+-driven stator (PomA/PotB) and a native Na^+-driven stator (PomA/PomB) were used in this study. Regarding the chimeric stator, we took an advantage of the PotB protein which consists of the N-terminal region of *V. alginolyticus* PomB and C-teminal region of *E.coli* MotB (Fig. 5A) and has been confirmed to function as a Na^+-driven stator when coexpressed with *V. alginolyticus* PomA in *E. coli* and in *Vibrio* (Asai *et al.*, 2003; Sowa *et al.*, 2005). Since this periplasmic region of PotB is derived from *E. coli* MotB which has a 91% similarity to the *Salmonella* $MotB_C$ (Zhu *et al.*, 2012), it is taken for granted that the structure information of *Salmonella* MotBc could be applied in the case of PotB. In particular, the linker region (residues 41-91) of PotB was deleted to simplify the protein structure to make sure that the remaining C-terminal region is exactly comprised of *E. coli* MotB. In this construct (named PotBΔL), the PEM region (known structure) is directly fused to the TM segment, but the construct was not functional. The motile suppressor was isolated from the strain expressing PotBΔL and we identified a mutation R109P (hereafter *E. coli* numeration for PotB residues in MotB region) that is responsible for restoring function. Following subsequent mutational and functional analyses in *E. coli* cell, we inferred that a conformational change in the α 1 helix specific for MotB/PomB protein restores the function of PotBΔL by the proper arrangement of TM segments and hence the Na^+-driven stator should share a similar mechanism (Fig. 5B)

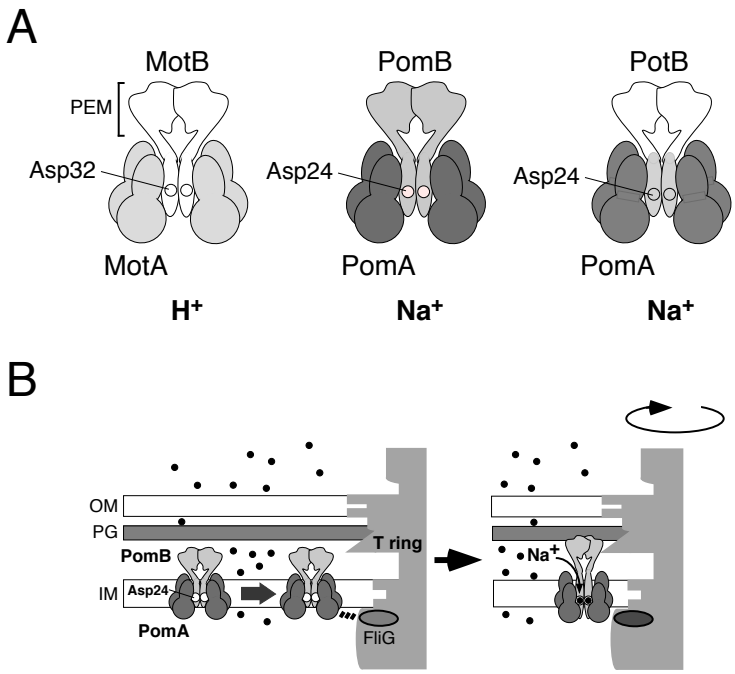

Fig. 5 (A) Schematic representation of the stator complex (the H^+-driven MotA/MotB complex of *E. coli*, the Na^+-driven PomA/PomB complex of *V. alginolyticus* and the Na^+-driven PomA/PotB chimeric stator complex). The essential charged residues for ion-binding and the PEM region are also shown in the figure. (B) A possible model for the PomA/PomB stator assembly around the polar flagellar motor of *V. alginolyticus* (Kojima *et al.*, 2011). When the PomA/PomB complex encounters the hook-basal body of the polar flagellum, FliG interacts with PomA (lines between PomA and FliG represent interaction) and this interaction induces a conformational change in the stator complex, allows Na^+ to translocate into the channel to reach Asp24 of the PomB and PGB domain of PomB to associate with the PG layer. At this stage, the T ring that is composed of MotX and MotY, may interact with the PGB domain of PomB and may help to stabilize the assembly of the Na^+-bound stator around the rotor. The bound Na^+ is then released from the complex, and torque is generated.

The native Na^+-driven stator is significantly different from the chimeric stator since it functions with the help of the T ring in the *Vibrio*. Without the T ring, the stator does not assemble around rotor and consequently flagellum does not rotate (Terashima *et al.*, 2006). Furthermore, a recent deletion study of the periplasmic region of PomB ($PomB_C$) revealed that PEM of PomB is about 30 residues (121-153) longer in the N-terminal side than that of $MotB_C$ (Fig. 6) (Li *et al.*, 2011). This extra residues and the following residues before the conserved OmpA-like region show no clear sequence similarity to MotB (Fig. 6). These finding imply that it has a distinctive mechanism from the chimeric Na^+-driven stator. To resolve this question, we purified and crystallized various fragments of $PomB_C$ and solved the structure of $PomB_{C4}$ (121-315) at a resolution of 2.3 Å (containing PEM), and $PomB_{C5}$ (135-315) at a resolution of 2.0 Å. Based on structure of $PomB_C$, an *in vivo* disulfide-crosslink study and motility assay revealed a novel insight into the molecular mechanism by which the stator couples sodium ion flow to flagellar rotation.

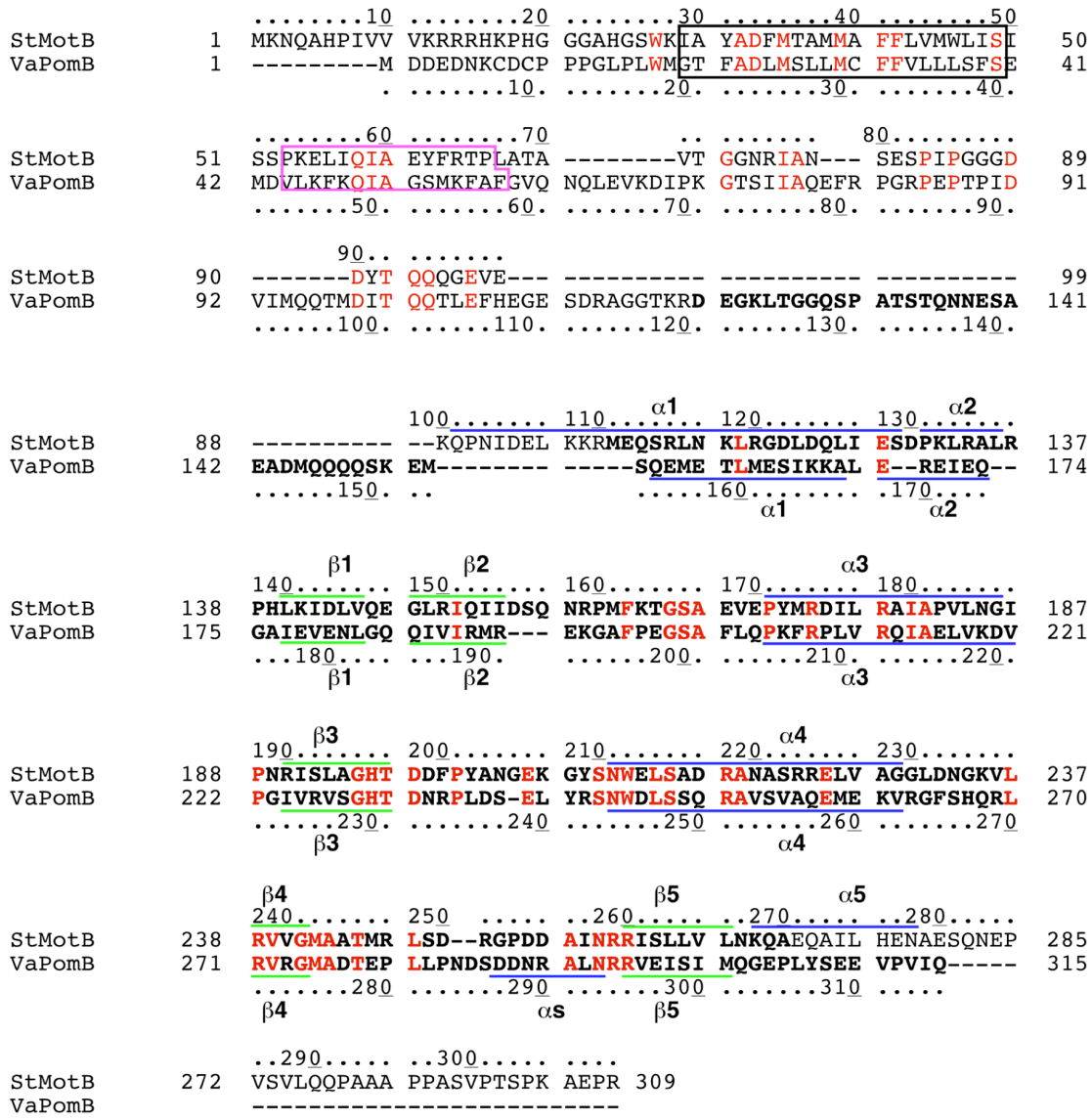

Fig. 6. Structural based sequence alignment of PomB and MotB.

The conserved residues are shown in red. The residues included in the PEM region are highlighted by bold characters. The secondary structure elements are shown below each sequence: blue line, α helix; green line, β strand. The tramsmembrane region and the plug region are indicated by black and magenta box, respectively.

Chapter2:

Functional analysis of stator activation of sodium-driven flagella

in *Escherichia coli*

Introduction

As mentioned in the Chapter 1, flagellar stator activation involves the periplasmic region of B subunit. The structural information of this region was unknown until recently when the periplasmic region of MotB ($MotB_C$) from *Helicobacter pylori* (Roujeinikova, 2008) and *Salmonella typhimurium* (Kojima *et al.*, 2009) was shown to have structures similar to a common OmpA-like fold, suggesting that stator can anchor in the PG layer. The *Salmonella* $MotB_C$ structure contains a PEM and it shows a single-domain structure with a long N-terminal a-helix that protrudes from the domain. Subsequent functional analyses suggest that this MotB-specific α-helix undergoes drastic conformational changes when the stator is incorporated into the motor. Together with the analyses of the plug, such conformational changes would allow the PEM region to be anchored around the rotor and to simultaneously open the channel to activate the proton-conducting activity. Similar mechanism is proposed in the Na^+-driven polar flagellar motor of *V. alginolyticus* (Fig. 5B) (Kojima *et al.*, 2011). However, experimental evidence for the conformational changes has not been reported yet and it still has not been experimentally investigated whether the Na^+-driven stator shares the same mechanism of activation with that of the H^+-driven stator.

In this study, to investigate how the Na^+-type stator is activated during the assembly step to the motor, we took advantage of the PotB protein. PotB is a fusion protein that consists of the N-terminal region of *V. alginolyticus* PomB and the C-terminal region of *E. coli* MotB (Fig. 7A), and can function as a Na^+-driven stator when co-expressed with *V. alginolyticus* PomA in *E. coli* or in *Vibrio* (Fig. 5A) (Asai *et al.*, 2003; Sowa *et al.*,

2005). Since its periplasmic region is derived from *E. coli* MotB, which has a 91% similarity to *Salmonella* MotB, it is taken for granted that the high-resolution structure of *Salmonella* $MotB_C$ (the PEM region) can be applied in the case of PotB. First, the linker region (residues 41-91) of PotB was deleted to simplify the protein structure to make sure that the remaining C-terminal region is exactly comprised of *E. coli* MotB. In this construct (named PotBΔL), the PEM region (known structure) is directly fused to the TM segment, but the construct was not functional. The motile suppressor was isolated from the strain expressing PotBΔL and we identified a mutation R109P (hereafter *E. coli* numeration for PotB residues in MotB region) that is responsible for restoring function. Following subsequent mutational and functional analyses, we speculate that a conformational change in the α1 helix specific for MotB/PomB protein affects the function of PotBΔL by the proper arrangement of TM segments that is required for the formation of a functional channel.

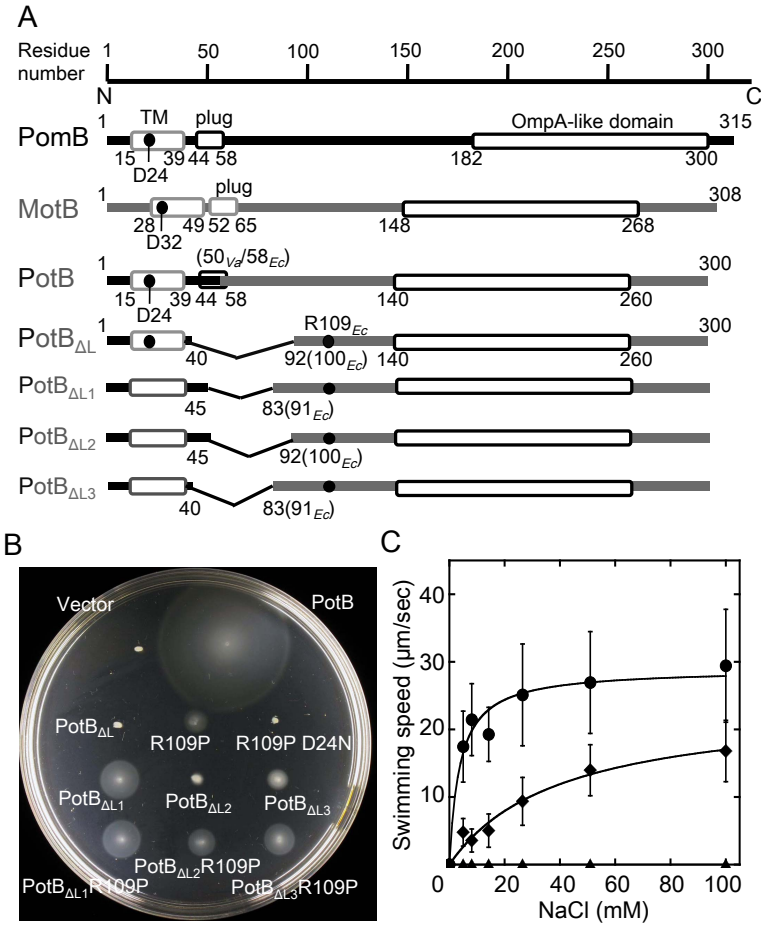

Fig. 7. The suppressor mutation restores the function of the stator.

(A) Schematic of the primary structures of PomB, MotB, PotB and PotB with different lengths of deletions in the linker region. The R109P point mutation was introduced into PotBΔL (Δ41-91), PotBΔL1 (Δ46-82), PotBΔL2 (Δ46-91) and PotBΔL3 (Δ41-82). All proteins have one TM domain and an OmpA-like domain, which is composed of about 120 residues. PotB contains a part of the N-terminal region of *Vibrio* PomB (residues 1 to 50) and the C-terminal region of *E. coli* MotB (residues 58 to 308). PotBΔL was constructed by deleting the linker region (residues 41 to 91) in PotB. (B) Motility assay of RP6894 cells harboring pACTrc (vector), pTSK4, pTSK45, pTSK45 R109P, pSZ3, pSZ4, pSZ5 and those with R109P mutation on TB soft agar plates containing 1 mM IPTG and 25 μg/ml chloramphenicol. Plates were incubated at 30°C for 8 hours. (C) Swimming speeds of RP6894 cells harboring pTSK4 (●), pTSK45 (▲) or pTSK45 R109P (◆). After 6 hours of culture, the cells were harvested, washed and suspended in various concentrations of NaCl in KPi buffer.

Results

A mutation in the N-terminal region of PEM restores the function of the linker-deleted PotB protein

Because *Salmonella* MotB with a deletion in the linker region (Δ51-100) can form a functional stator complex with MotA, and its overproduction does not impair the growth of the host cell (Muramoto and Macnab, 1998), at first we examined whether the PotB construct with a similar deletion (Δ41-91, hereafter named PotBΔL, Fig. 7A) was functional or not. A His_6-tag was attached to the C-terminus of PotB and PotBΔL, and these constructs were co-expressed with PomA from an IPTG-inducible plasmid pTSK45 in the *E. coli* Δ*motAB* strain RP6894. This *E. coli* strain producing PotBΔL-His_6 with PomA did not form motility ring on the soft-agar plate as seen to those without the stator complex (Fig. 7B). This was confirmed by dark-field microscopy, where no motile cells were observed (data not shown). The PotBΔL protein could be detected by the immunoblot of the whole cell lysate, but with significantly smaller amount compared to the full-length PotB (Fig. 8A). It seems unlikely that the low level of PotBΔL protein in the cell is critical for motor function, since overproduction of PotBΔL by a higher concentration of IPTG (10 mM) did not improve motility. We succeeded in isolating a spontaneous motile revertant from this nonmotile strain as a small motility halo following prolonged incubation (24 hours) on soft-agar plate. We confirmed that the suppressor mutation was on the plasmid, and then sequencing results revealed that the restoration of the stator function was attributed to a replacement of Arg at position 109 (*E. coli* MotB numeration) with Pro in the MotB

region of PotB. It might be noteworthy that typical Arg codons (CGX) are more likely to mutate to Pro (CCX), just to have C as their second base. This suppressor hunting was independently repeated, and we again identified the R109P replacement in the isolated suppressor. PotBΔL (R109P) protein was detected by the immunoblot as similar level to the full-length PotB (Fig. 8A).

To test whether the length of the deletion is the cause for the non-functionality of the PomA/PotBΔL stator, we constructed deletion mutants of PotB which have an N- or C-terminal extension(s) to PotBΔL: PotBΔL1 (Δ46-82), PotBΔL2 (Δ46-91) and PotBΔL3 (Δ41-82) (Fig. 7A and B). Cells producing the mutant with the shortest deletion (PotBΔL1) formed a motility ring similar to that of PotBΔL(R109P), while the slightly longer deletion in PotBΔL3 led to a smaller motility ring (Fig. 7B). In the case of PotBΔL2, in which the deletion was only 5 amino acids shorter than in PotBΔL, no motility ring was observed (Fig. 7B), but when observed under the dark-field microscopy we could find a few motile cells. We also examined the effect of R109P mutation on the function of these shorter deletion constructs (Fig. 7B). R109P mutation did not affect the motility of the cells expressing the PomA/PotBΔL1 stator, in contrast to other mutants. These results suggest that the re-insertion of residues at the deleted part of the PotBΔL protein (by shortening the deletion) has a similar effect on the function of the stator as R109P mutation does.

We measured swimming speed of the cells expressing PomA/PotBΔL(R109P) stator complex, and confirmed that its motility depended on the Na^+ concentration of the medium, indicated that the PomA/PotBΔL(R109P) complex functions as a Na^+-driven

stator (Fig. 7C). Then, the degree of interaction between PomA and PotB (mutants) was examined by using the co-elution assay (Fig. 9) by using a His-tag attached to the C-terminus of PotB, PotBΔL and PotBΔL(R109P). The results show that compared to the wild type, ΔL deletion reduced about 64% amount of co-eluted PomA with PotB, and this weakened interaction due to the ΔL deletion was not enhanced by the R109P mutation. These results indicate that the non-functionality of the PomA/PotBΔL stator is not caused by lower level of protein or the disruption of the interaction between PomA and PotB.

The effect of the over-production of the mutants on cell growth

To confirm whether the mutation will affect the ion channel comprised of PomA and PotBΔL proteins, the growth of cells over-expressing these mutant stators was monitored (Fig. 10). As already mentioned, segments consisting of residues from P52 to P65 in *E. coli* MotB and those from V44 to F58 in *V. alginolyticus* PomB are considered as plug segments for the H^+ or Na^+ channels (Hosking *et al.*, 2006; Li *et al.*, 2011), and if these residues are deleted, overproduction of mutant stators cause severe growth impairment. Our results showed that the overproduction of PomA/PotBΔL does not affect the host cell growth, even though residues 41- 91 (- 99, of *E. coli* numeration) which include the plug segment in the PotB region are deleted (Fig. 10A). In contrast, the over-production of PotBΔL(R109P) with PomA drastically hindered the growth of host *E. coli* cells (Fig. 10A). Furthermore, as our previous study reported (Li *et al.*, 2011), the additional mutation (D24N of PomB) that disrupts the critical Na^+ binding

site of the stator eliminated the growth inhibition of the cells expressing the PomA/PotBΔL(R109P) stator (Fig. 8A) without affecting protein stability or expression (Fig. 8A). We did these growth experiments by using the *E. coli* DH5α as a host strain (Fig. 10), and similar growth inhibition was also observed when the PomA/PotBΔL(R109P) complex was overproduced in another strain RP3098, which does not express any flagellar proteins, or in the strain RP6894 (Δ*motAB*) (data not shown). Similarly, all PotB mutants with shorter deletion constructs of PotB and those with the R109P mutation caused significant growth inhibition, which is likely to be associated with the level of function (Fig. 10B).

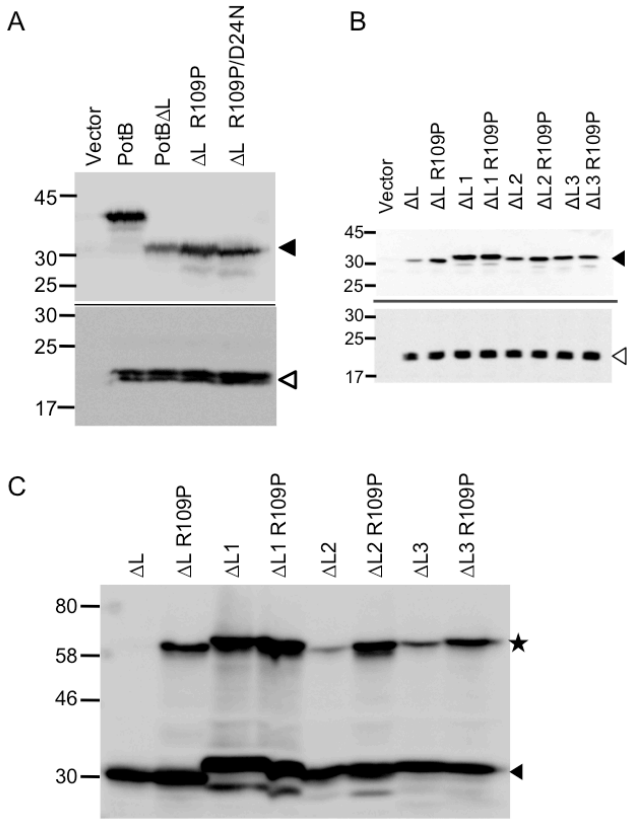

Fig. 8. (A) Immunoblot analysis of mutant stator proteins. RP6894 cells harboring the plasmids noted were cultured in LB medium at 37ºC for 4 hours. Proteins from whole cell extracts were analyzed by immunoblotting using an anti-PomA antibody (lower panel) and an anti-*Salmonella* $MotB_C$ antibody (upper panel). Open and closed triangles represent PomA and PotBΔL, respectively. (B) Immunoblot analysis of mutant stator protein. RP6894 cells harboring the plasmids noted were cultured in TG medium at 30ºC for 6 hours. The whole-cell extracts were analyzed by SDS-PAGE followed by immunoblotting with an anti-PomA antibody (lower panel) and an anti-*Salmonella* $MotB_C$ antibody (upper panel). Open and closed triangles represent PomA and PotBΔL, respectively. (C) Disulfide crosslinking of internal *potB* deletion mutants. PotBΔL (Δ41-91), PotBΔL1 (Δ46-82), PotBΔL2 (Δ46-91), PotBΔL3 (Δ41-82) and those with R109P mutations were examined as Fig. 3A. RP6894 cells harboring the plasmids noted were grown in TG medium containing 1 mM IPTG and 25 μg/ml chloramphenicol and were collected after 6.5 hours. Proteins in the whole-cell extracts were separated by SDS-PAGE in the absence of β-mercaptoethanol, and PotB proteins were detected by immunoblot using an anti-*Salmonella* $MotB_C$ antibody. The cross-linked dimer (★) and monomer (▲) of PotB are indicated, respectively.

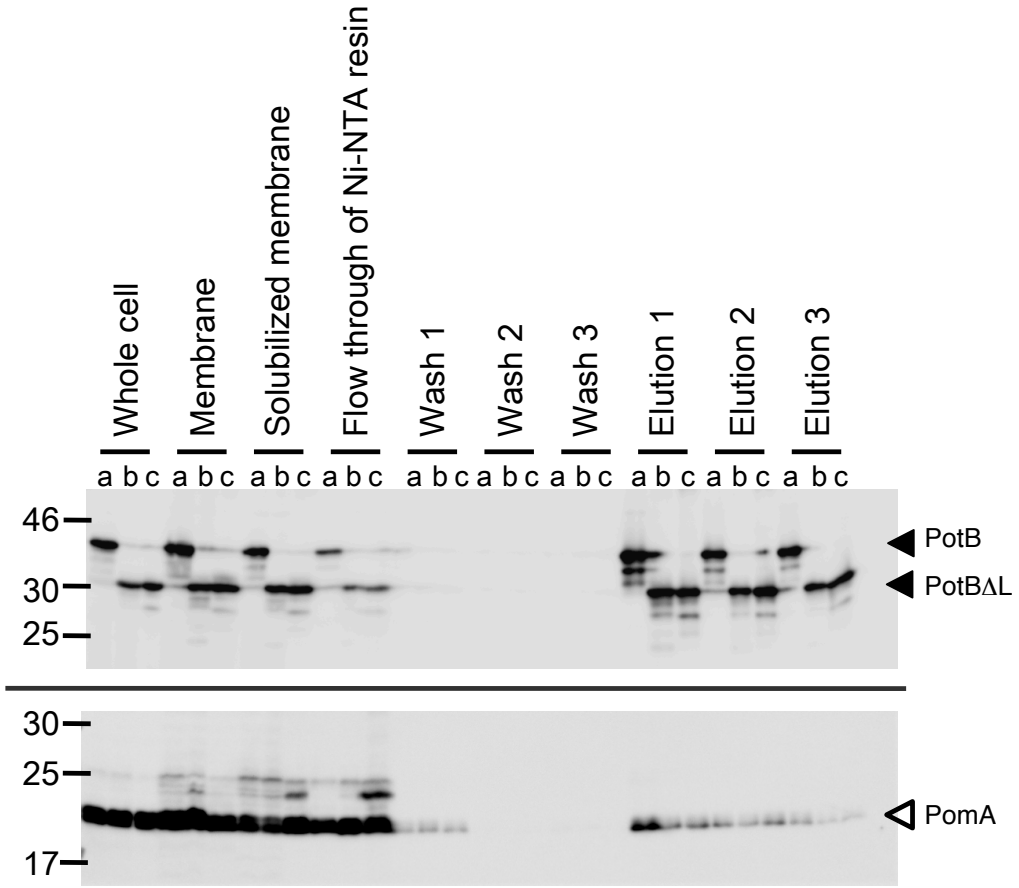

Fig. 9. The interaction between PomA and PotB is partially reduced due to the Δ L deletion, but the mutation R109P does not affect that interaction.

In each fraction, PomA/PotB (lane a), PomA/PotBΔL (lane b) and PomA/PotBΔL R109P (lane c) were loaded in sequence from left to right. PomA/PotB-His_6 and its derivatives were expressed from the respective plasmids (pTSK4 for PomA/PotB, pTSK45 for PomA/PotB Δ L and its R109P derivative), by 1 mM IPTG in RP6894 cells cultured 6 hours in TG medium. Co-elution assay was carried out as described previously (Takekawa *et al.*, 2012), by using a detergent Cymal-5 for solubilization. All samples were analyzed by SDS-PAGE followed by immunoblotting with an anti-PomA antibody (lower panel) and an anti-*Salmonella* $MotB_C$ antibody (upper panel). Open and closed triangles represent PomA and PotB of stator complex, respectively.

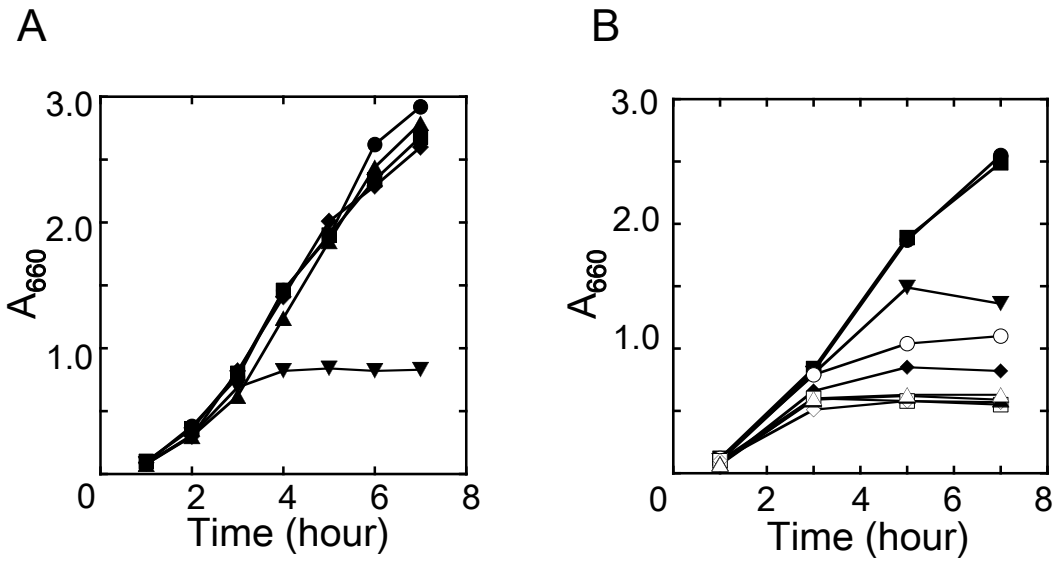

Fig. 10. The effect of PotBΔL R109P and relative mutants over-production on cell growth.

(A) DH5α cells harboring pACTrc (●), pTSK4 (■) pTSK45(◆), pTSK45-R109P(▼) or pTSK45-R109P D24N (▲) were grown in LB medium containing 25 μg/ml chloramphenicol and 1 mM IPTG at 37℃ for 8 hours. Cell growth was monitored by measuring the absorbance of 660 nm at every hour interval. (B) Cell growth of DH5α cells harboring vector (●), pTSK45 (PotBΔL, ■), pSZ3 (PotBΔL1, ◆), pSZ4 (PotBΔL2, ▼), pSZ5 (PotBΔL3, ○), pTSK45 R109P (□), pSZ3 R109P (◇), pSZ4 R109P (▲) or pSZ5 R109P (△). Overnight cultures were inoculated at a 1:100 dilution in LB medium containing 1 mM IPTG and 25 μg/ml chloramphenicol and were incubated for 8 hours in a shaker at 37ºC. OD_{660} values were monitored at hourly intervals.

Mutations of residue Arg 109 of PotBΔL and Proline scanning of adjacent residues around R109

Proline is known to act as a structural disruptor when in the middle of α-helices and β-sheets (Moradi *et al.*, 2009). To learn more about the requirements other than Pro for the function at residue 109 of PotBΔL, replacements of R109 with L, A, W (with hydrophobic side chain), D and E (with negative charged side chain), K (with positive charged side chain), C and S (with polar uncharged side chain) were introduced, and to examine their motility, these mutants of PotBΔL were co-expressed with PomA from the plasmid pTSK45 in the Δ*motAB* strain RP6894. Charged and polar mutations (R109D, R109E) gave a similar size of the motility ring to that of R109P, and R109S showed a slightly smaller ring (Fig. 11A). From the observation by a dark field microscopy, cells expressing the PomA/PotBΔL stator with mutations of R109A, R109W or R109C could be shown to be very weakly motile, but those with the mutations of R109L or R109K were non-motile (data not shown). Growth inhibition was only induced in functional mutants (Fig. 11B). Immunoblot analysis showed that the expression of R109D, R109E, R109A or R109S mutant proteins were detected twice higher levels than others, although the PomA level was not affected by those mutations (Fig. 11C). The level of the mutant PotBΔL protein is correlated to the stator function.

To investigate whether mutations in the adjacent residues around R109 can also affect the functioning of the PomA/PotBΔL stator, we scanned residues 105 to 113 (*E. coli* numeration) with Pro, all of which are located in the middle of the α1 helix connected to the PG-binding domain based on the crystal structure of *Salmonella* $MotB_C$. Cells

co-expressing PomA and the mutants PotBΔL with the E105P, Q112P or S113P mutations did not form motility rings (Fig. 12A). However, other mutants showed motility, as well as growth inhibition (Fig. 12B). Immunoblot analysis showed a slightly higher level compared to nonfunctional one, again the protein level is correlated to the stator function (Fig. 12C). Based on these results, we speculate that Pro replacements at residues from 106 to 111 alter the conformation of the N-terminal PEM region, and such conformational change restores the function of PotBΔL.

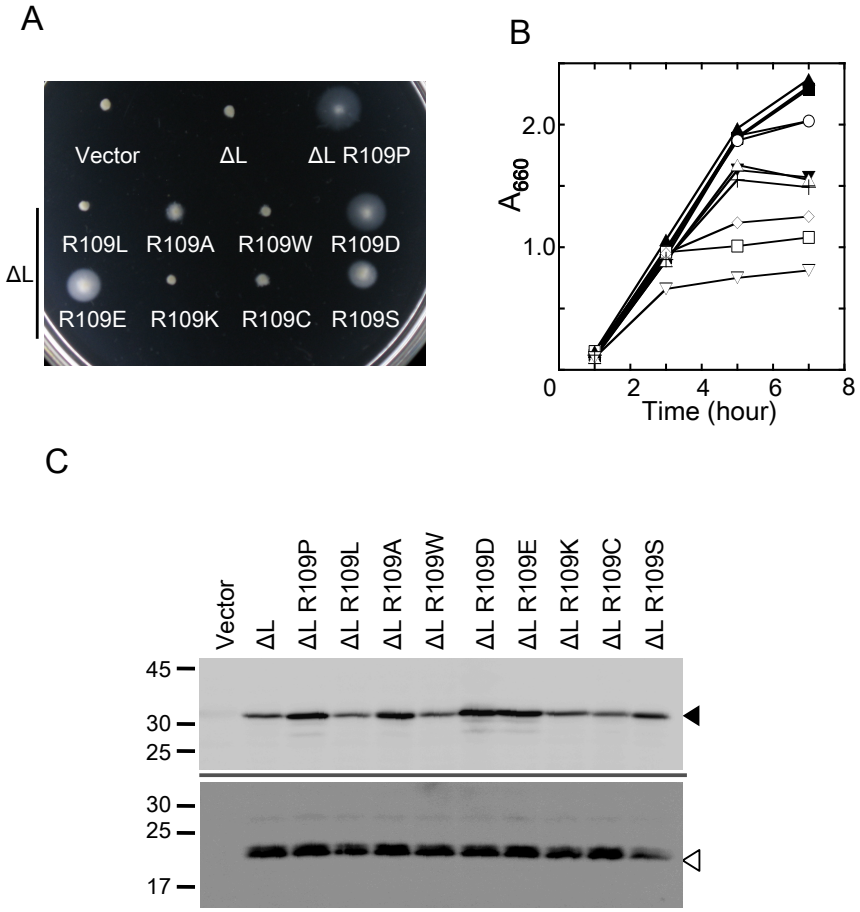

Fig. 11. Effects of various substitutions at residue Arg109.

(A) Motility assay of RP6894 cells harboring pACTrc (Vector), pTSK45(ΔL), pTSK45 R109P, R109L, R109A, R109W, R109D, R109E, R109K, R109C or R109S on TB soft agar plates containing 1 mM IPTG and 25 μg/ml chloramphenicol. Plates were incubated at 30ºC for 20 hours. (B) Cell growth of DH5α cells harboring pACTrc (●), pTSK45 (■), pTSK45 R109P (▽), pTSK45 R109L (◆), pTSK45 R109A (▼), pTSK45R109W (○), pTSK45R109D (□), pTSK45 R109E (◇), pTSK45 R109K (▲), pTSK45 R109C (△) or pTSK45 R109S (+). Cells were grown in the LB medium containing 25 μg/ml chloramphenicol and 1 mM IPTG at 37ºC for 8 hours. OD_{660} values were monitored at hourly intervals. (C) Immunoblot analysis of mutant stator proteins. RP6894 cells harboring the plasmids noted above were grown in the TG medium at 30ºC for 6 hours. The whole-cell extracts were analyzed by SDS-PAGE followed by immunoblotting with an anti-PomA antibody (lower panel) and an anti-*Salmonella* $MotB_C$ antibody (upper panel). Open and closed triangles represent PomA and PotBΔL, respectively.

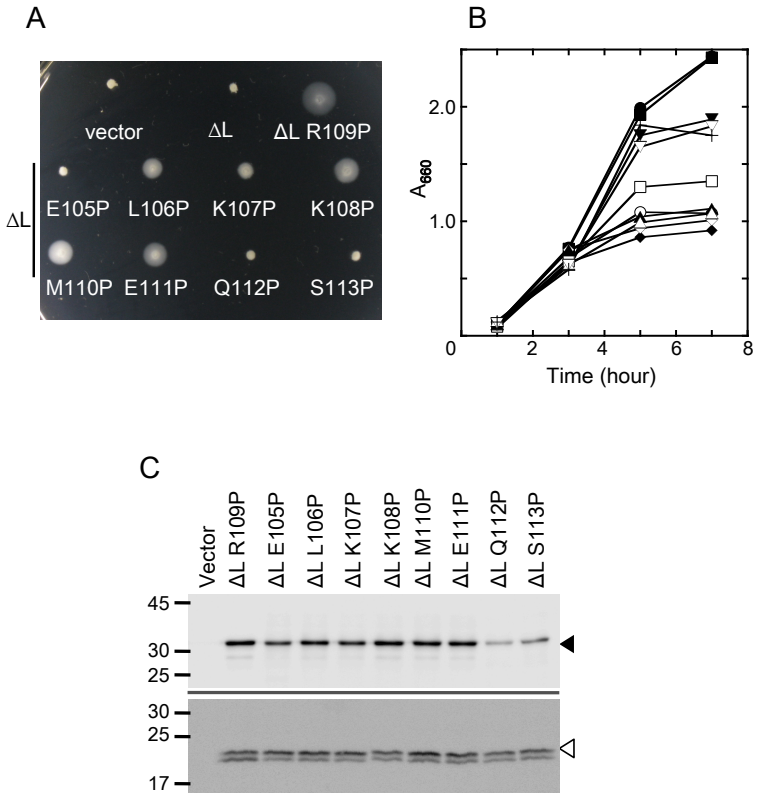

Fig. 12. Scanning of Pro substitutions in the vicinity of Arg109.

(A) Motility of RP6894 cells harboring pACTrc (vector), pTSK45 (ΔL) or pTSK45 with respective mutations in PotBΔL. Motility was examined on soft agar TG plates containing 1 mM IPTG and 25 μg/ml chloramphenicol at 30ºC for 20 hours. (B) Growth inhibition of cells producing mutant stator proteins. Overnight culture of DH5α cells containing pACTrc (●), pTSK45 (■), pTSK45 R109P (◆), pTSK45 E105P (▼), pTSK45 L106P (○), pTSK45 K107P (□), pTSK45 K108P (◇), pTSK45 M110P (▲), pTSK45 E111P (△), pTSK45 Q112P (▽) or pTSK45 S113P (+) were inoculated at a 100-fold dilution in LB medium containing 1 mM IPTG and 25 μg/ml chloramphenicol and were incubated for 8 hours with shaking at 37ºC. OD_{660} values were monitored at hourly intervals. (C) Immunoblot analysis of mutant stator proteins. RP6894 cells harboring the plasmids noted were grown in TG medium containing 1 mM IPTG and 25 μg/ml chloramphenicol at 30ºC for 6 hours. The whole-cell extracts were analyzed by SDS-PAGE followed by immunoblotting with an anti-PomA antibody (lower panel) and an anti-*Salmonella* $MotB_C$ antibody (upper panel). Open and closed triangles represent PomA and PotBΔL, respectively.

Detection of disulfide bridge formation near the TM segment of PotBΔL

PomB has three cysteine residues in its N-terminus (C8, C10 and C31), and C8 and C10, which are located near the cytoplasmic end of the single TM segment of PomB, are involved in the disulfide bridge formations in the wild-type PomB dimer (Yorimitsu *et al.*, 2004). Thus, the formation of such a bridge could reflect the proper arrangement of the TM segments of PomB or PotB, that is required for the formation of a functional channel. Non-reducing SDS-PAGE analysis showed that the functional PotBΔL mutants have the ability to form a dimer via disulfide bridge(s) between these cysteines as seen in the wild-type PotB (Fig. 13A, the upper panel). Efficiency to form the disulfide bridge was correlated to the level of PotBΔL function: dimer formation of weakly functional PotBΔL(R109S) was reduced as compared to PotBΔL(R109P or R109D), and very lower level of dimer band was detected for nonfunctional PotBΔL and PotBΔL(R109L). Reducing SDS-PAGE showed the lower protein levels for the non-functioning PotBΔL, suggesting that reduced dimer band could be caused by lower protein level in the cell. However such a possibility is unlikely, because the dimer band was still quite weak even when we loaded twice more amount of these nonfunctional PotBΔL on the gel (Fig. 13A, right-most 3 lanes). These results suggest that the proper arrangement of the N-terminal region of nonfunctional PotBΔL is disrupted and hence affected their function.

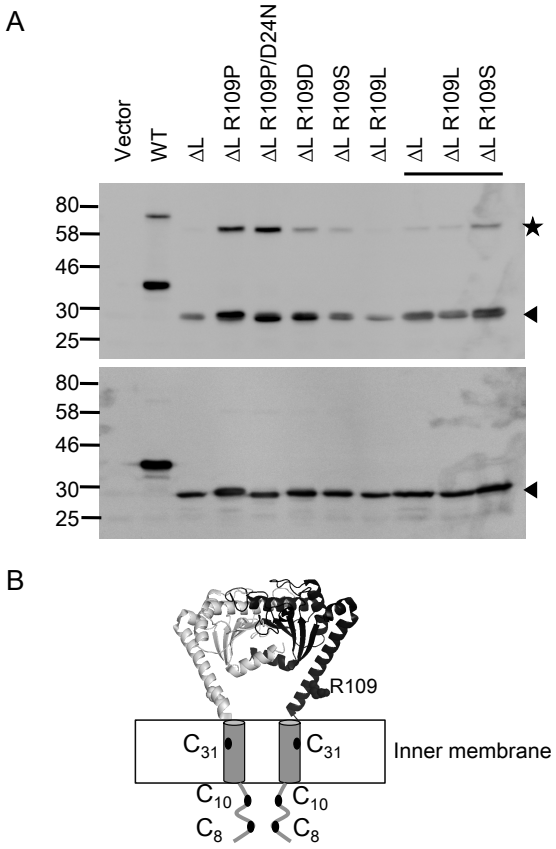

Fig. 13. Disulfide-crosslinking of PotB, PotBΔL and its mutants.

RP6894 cells harboring the plasmids noted were grown in TG medium containing 1 mM IPTG and 25 μg/ml chloramphenicol and were collected after 6.5 hours. Proteins in the whole-cell extracts were separated by SDS-PAGE in the absence (upper panel) or presence (lower panel) of β-mercaptoethanol and PotB or PotBΔL proteins were detected by immunoblot using an anti-*Salmonella* $MotB_C$ antibody. Note that at the right-most three lanes samples were twice the volume of the other lanes. The cross-linked dimer and monomer of PotBΔL are shown as ⋆ and shown as that. WT: wild-type PotB, L: PotBΔL. (B) A model of PotBΔL structure. The periplasmic part of the structure shows the crystal structure of the C-terminal periplasmic region of *Salmonella* MotB (2ZVY) (Kojima *et al.*, 2009). PotBΔL forms a dimer, each subunit of which is shown in gray or black. The Arg 109 is indicated by the black sphere. Three cysteine residues in PotBΔL are also shown in the model. C8 and/or C10 are involved in disulfide bridge formation. Deletion of the linker (Δ41-91) of PotB disrupts disulfide bridge formation, but the additional mutation R109P restored the crosslink.

Discussion

In this study, based on the structural information of $MotB_{C2}$, an internal deletion mutant of PotB (PotBΔL) was constructed, which lacks a linker region that connects the single TM segment and the PEM region to investigate the activation of Na^+-driven stator. Similar deletion mutants in *Salmonella* MotB or *Vibrio* PomB were functional (Muramoto and Macnab, 1998; Kojima *et al.*, 2009; Li *et al.*, 2011), but that turned out not to be the case for PotB. By isolating a motile suppressor mutant from the non-motile PotBΔL strain, the R109P mutation (*E. coli* numeration) was identified. Arg109 is located on the α1-helix of the *Salmonella* $MotB_{C2}$ structure. The ΔL deletion affects protein amount in the cell and weakens PomA-PotB interaction, but these effects do not abolish the function of PotB, since overproduction of PotBΔL by a higher concentration of IPTG (10 mM instead of 1 mM) did not restore motility of the cells and R109P mutation did not affect the amount of PomA co-isolated with His-tagged PotBΔL (Fig. 9). Furthermore, disulfide bridge formation PotBΔL via the N-terminal cysteine residues was greatly reduced as discussed later, so we conclude that ΔL deletion disrupt the function of PomA/PotB stator and the R109P mutation suppresses the mutational effect.

The fact that the suppressor mutation was mapped on the helix α1 of *Salmonella* $MotB_C$ structure is intriguing since previous structure-based functional analyses of $MotB_C$ in *Salmonella* showed that a mutation in this helix (L119P or E) alters the conformation of the stator complex to allow efficient assembly around the motor and proton translocation, and the secondary structure prediction of various MotB/PomB

proteins showed that this helix seems to be common for these proteins (Kojima *et al.*, 2009). Thus, it is plausible for PotBΔL that the N-terminal PEM region also forms a long helix as reported in the crystal structure, and that the R109P mutation alters the conformation of this helix needed to optimize the PotBΔL structure for function. This idea is supported by the fact that shorter deletions retained PotB function (Fig. 7B). Since an additional 10 amino acid deletion from PotBΔL1 resulted in a nonfunctional PotBΔL2, and the R109P mutation did not significantly affect the function of PotBΔL1 but restored the function of PotBΔL2, we speculate that a proper inter-domain connection between the TM segment and the PEM region is required for function, and the R109P mutation may act to relieve the steric hindrance at the inter-domain connection of PotBΔL so as to restore function. Our results could be interpreted in the way that a too-short linker in PotBΔL introduces tension that disrupts the TM parts of the stator, and anything that relaxes this tension (including point mutations that tend to relax the helical structure or introduce a point of flexibility) could then restore function. In this case, the region of the protein around residue 109 is not necessary to play a specific role for stator function. But we still argue the importance of the region R109 since (i) two independent suppressor hunting resulted in the isolation of identical R109P mutation, (ii) an introduction of L118E mutation to the full length PotB caused severe reduction of protein level so a mutation in helix α1 apart from the region around R109 may not restore function of PotBΔL, (iii) the swimming speed of full-length PotB with R109P mutation is about 1.4 times faster than that of wild type at 100 mM NaCl (40 μm/sec for PotB(R109P) and 28 μm/sec for PotB).

Subsequent results of mutational analyses at residue 109 showing that negatively charged (Asp, Glu) or polar side chains (Ser) at this position restore the function of PotBΔL (Fig. 11A), enable us to speculate that an insertion of a negative charge or a structurally restrained residue at position 109 disrupts or partially unfolds the helix structure so that the mutations mentioned above relieve the steric hindrance because of a linker deletion of PotB. Alternatively, since the side chain of Arg109 is exposed to the surface and is pointed outside of the *Salmonella* $MotB_{C2}$ dimer in the structure, it is possible that the region including Arg109 may interact with other protein surface(s) and that such interactions inhibit PotBΔL function. PomA could be the candidate as an interacting partner at the surface around Arg109 since the periplasmic segments of PomA contain several Asp residues. However, our Pro-scanning mutagenesis analysis revealed that not a specific but nearby residues of Arg109 allow Pro replacement to restore PotBΔL function (Fig. 12A), which suggests that a global conformational change at the helix seems to be induced by the mutation. Therefore we favor the first possibility noted above. To resolve this, we need to investigate the structure of the N-terminal PEM of PotBΔL with or without the R109P mutation.

It has been shown that wild-type PomB forms a cross-linked dimer by Cys 8 and/or Cys 10, residues that are located in the cytoplasmic region and are close to the TM helices (Yorimitsu *et al.*, 2004). This led us to observe the disulfide crosslink to investigate the arrangement of TM segments of PotBΔL. Our results clearly indicate that the function of stator is correlated to an ability to form the crosslink in PotB (Fig. 13). The mutation R109P strengthens not only the formation of ΔL monomer but also

the formation of disulfide crosslink (Fig. 13A), and the R109S mutant, that slightly lower function as compared to R109P (Fig. 11A), showed the similar level of ΔL monomer but the formation of cross-linked dimer was reduced. These results suggest the deletion of residues 41 to 91 in PotB enforces the abnormal arrangement of TM segments in the stator complex that impairs proper formation of the channel pore. We speculate that the R109P and other functional mutations induce a conformational change of the N-terminal PEM region of PotBΔL that relocates the TM helix to an appropriate place so as to restore function.

PotBΔL as well as PotB did not affect growth when overproduced, although PotBΔL lacks a plug segment. On the other hand, PotBΔL(R109P) did cause growth impairment. We assume that the growth impairment is caused by the massive Na^+ influx through the mutant stator complex, since a mutation that abolishes Na^+ binding to the stator (PotB D24N) eliminates the growth impairment without affecting formation of cross-linked dimer (Fig. 10A and Fig. 13A). In the plug-deleted PomB case, measured intracellular Na^+ concentrations confirmed that over-production of the plug-deleted stator causes higher Na^+ accumulation as compared to the wild-type stator (Takekawa *et al.*, 2013). It is noteworthy that all functional mutants have ability to form the disulfide bridge (Fig. 13 and Fig. 9C), and their overproduction inhibits the growth of host cells. The degree of inhibition is mostly in accordance with the level of dimer formation and motility (Fig. 8C, Fig. 10 and Fig. 13). How Na^+ at a higher concentration affects the cell physiology of *E. coli* is not clear, but from these results we assume that the mutant stator, PomA/PotBΔL R109P, is an active form of stator that conducts Na^+ efficiently.

Recently, it has been shown that interaction between the cytoplasmic region of a stator (MotA or PomA) and the rotor component FliG is necessary for activation of the stator complex (Fig. 5B) (Morimoto *et al.*, 2010b; Kojima *et al.*, 2011; Takekawa *et al.*, 2012). The current model for H^+-driven stator assembly and activation proposed that this rotor-stator interaction triggers conformational changes in the N-terminal region of PEM that open the stator channel and allow the PG-binding domain to anchor to the PG layer (Kojima *et al.*, 2009; Kojima *et al.*, 2011; Li *et al.*, 2011). Our results show that the mutation in helix α1 of $MotB_C$ restores the function of the Na^+-driven PotBΔL stator protein and that mutant (R109P) in an active state as shown by growth impairment, and these facts are not in conflict, but are complementary with the model about the assembly of H^+-driven stator proposed earlier. Furthermore, our Pro-scanning and localized mutagenesis studies suggest that the structural alteration in helix α1 of PotBΔL might be induced, probably by its unfolding, to produce functional stator as an active form. These results support and further emphasize the functional importance of the helix α1, to activate ion-translocation activity and to anchor at the PG layer when the stator is incorporated into the motor. A recent crystallographic analysis of a longer $MotB_C$ fragment of *Helicobacter pylori* showed that the linker sequence (residues 64-112) is separated from the conserved PG-binding core domain (O'Neill *et al.*, 2011), so that is also consistent with the model of stator assembly and activation described above. Concerning conformational changes coupling to stator assembly and activation, we are currently attempting to crystallize $MotB_C$ fragments with mutations in the α1 helix. The high-resolution structures of those fragments will give us detailed insights into the

mechanism of assembly-coupled stator activation, and most importantly, insights into the properties of the active stator that is competent to generate torque.

Material and Method

Bacterial strains, plasmids and mutagenesis

Bacterial strains and plasmids used in this study are listed in the Table 1. The DNA sequence encoding for the frame of *pomA* and *potB* with the His_6 tag was amplified by PCR, and cloned into the NdeI and BamHI sites of pACTrc to construct pTSK4. The in-frame deletion of PotB was carried out using a one-step-PCR-based method as described previously (Li *et al.*, 2011), with the plasmid pTSK4 as a template. Therefore, in this study, stator proteins including mutants were expressed under the control of the IPTG-inducible *trc* promoter. Point mutations on the PotBΔL protein were generated using the plasmid pTSK45 (encoding for *pomApotBΔL*) as a template and the QuikChange site-directed mutagenesis protocol (Stratagene). All plasmids carriy the chloramphenicol resistance. All mutations and in-frame deletions were confirmed by DNA sequencing with an ABI Prism 3130 genetic analyzer (Applied Biosystems).

Motility assay on soft agar plates

In all experiments, we inoculated fresh individual colonies on soft agar plates. Colonies of *E. coli* strains harboring vectors or respective plasmids were formed overnight at 37ºC on LB-Cm plates (1% Bacto Trypton, 0.5% Yeast Extract, 0.5% NaCl, 1.25% agar, 25 μg/ml chloramphenicol). Those colonies were picked by toothsticks and inoculated on the surface of TB soft agar plates (1% Bacto Trypton, 0.5% NaCl, 0.28% agar, 25 μg/ml chloramphenicol) including 1 mM isopropyl-β-D-thiogalactoside (IPTG).

The plates were incubated at 30℃ for 20 hours to form motility rings.

Measurement of swimming speeds

Cells were cultured overnight in LB medium at 37ºC and were then diluted 100-fold into TG medium (1% Bacto Trypton, 1% glycerol, 0.5% NaCl) containing 25 μg/ml chloramphenicol and 1 mM IPTG. After this, they were re-cultured at 30ºC for at least 4 hours. Cells were harvested by centrifugation and were washed twice with the KPi buffer (pH 7.6, potassium phosphate buffer, 10 mM DL-lactic acid) containing 100 mM NaCl. The washed cells were resuspended in the KPi buffer containing various concentrations of NaCl (from 0 mM to 100 mM), to which serine was then immediately added to a final concentration of 20 mM to suppress directional changes of swimming cells. The motility was observed under a dark-field microscopy and was recorded on a video tape. The swimming speeds of cells were analyzed by a software (Move-tr/2D, Library Co., Tokyo, Japan) as described previously (Terauchi *et al.*, 2011).

Growth curves

E. coli cells (DH5α) harboring plasmids were cultured overnight at 37°C in LB medium containing 25 μg/ml chloramphenicol. The overnight cultures were diluted 100-fold into 3 ml LB medium containing 25 μg/ml chloramphenicol and 1 mM IPTG, and were cultured for 8 hours with shaking. Cell densities were monitored at OD_{660} at hourly intervals.

Immunoblot analysis of whole cell extracts

The overnight cultures in LB medium (for Fig 9A) or TG medium (for Fig 13A, Fig. 9B and 9C, Fig. 10, Fig. 11C and Fig. 12C) for detecting motility of RP6894 cells harboring plasmids were diluted 1:100 in 10 mL medium containing 25 μg/ml chloramphenicol and 1 mM IPTG and were incubated under shaking at 37°C for 4 hours (LB medium) and at 30°C for 6 hours (TG medium). All cells were collected when they reached the log phase of growth and were re-suspended to an OD_{660} of 10 in an SDS loading buffer with or without β-mercaptoethanol. After boiling the mixture at 95°C for 5 min, proteins were separated by SDS-PAGE and immunoblotting was carried out as previously described (Terauchi *et al.*, 2011) using an anti-PomA1312 antibody (Yorimitsu *et al.*, 1999) for the detection of PomA and an anti-*Salmonella* MotB antibody (Kojima *et al.*, 2008a) for the detection of PotB or PotBΔL. Protein levels were not significantly affected by the difference of culture medium (LB or TG).

Table 1

Strain or plasmid	Description	Source or reference
E. coli strain		
DH5α	Recipient for cloning experiments	
RP6894	Δ*motAB*	(Slocum and Parkinson, 1983)
Plasmid		
pACTrc	pACYC-184 based plasmid, *trc* promoter, Cm^r	G. M. Fraser
pTSK4	pACTrc/PomA+PotB-His_6	This study
pTSK45	pACTrc /PomA+PotB Δ L(Δ 41-91) -His_6	This study
pTSK45-R109P	pACTrc /PomA+PotB Δ L(Δ 41-91, R109P) -His_6	This study
pTSK45-R109L	pACTrc /PomA+PotB Δ L(Δ 41-91, R109L) -His_6	This study
pTSK45-R109A	pACTrc /PomA+PotB Δ L(Δ 41-91, R109A) -His_6	This study
pTSK45-R109W	pACTrc /PomA+PotB Δ L(Δ 41-91, R109W) -His_6	This study
pTSK45-R109D	pACTrc /PomA+PotB Δ L(Δ 41-91, R109D) -His_6	This study
pTSK45-R109E	pACTrc /PomA+PotB Δ L(Δ 41-91, R109E) -His_6	This study
pTSK45-R109K	pACTrc /PomA+PotB Δ L(Δ 41-91, R109K) -His_6	This study
pTSK45-R109C	pACTrc /PomA+PotB Δ L(Δ 41-91, R109C) -His_6	This study
pTSK45-R109S	pACTrc /PomA+PotB Δ L(Δ 41-91, R109S) -His_6	This study
pTSK45-E105P	pACTrc /PomA+PotB Δ L(Δ 41-91, E105P) -His_6	This study
pTSK45-L106P	pACTrc /PomA+PotB Δ L(Δ 41-91, L106P) -His_6	This study
pTSK45-K107P	pACTrc /PomA+PotB Δ L(Δ 41-91, K107P) -His_6	This study
pTSK45-K108P	pACTrc /PomA+PotB Δ L(Δ 41-91, R108P) -His_6	This study
pTSK45-M110P	pACTrc /PomA+PotB Δ L(Δ 41-91, M110P) -His_6	This study
pTSK45-E111P	pACTrc /PomA+PotB Δ L(Δ 41-91, E111P) -His_6	This study
pTSK45-Q112P	pACTrc /PomA+PotB Δ L(Δ 41-91, Q112P) -His_6	This study
pTSK45-S113P	pACTrc /PomA+PotB Δ L(Δ 41-91, S113P) -His_6	This study
pSZ3	pACTrc /PomA+PotB Δ L1(Δ 46-82) -His_6	This study
pSZ4	pACTrc /PomA+PotB Δ L2(Δ 46-91) -His_6	This study
pSZ5	pACTrc /PomA+PotB Δ L3(Δ 41-82) -His_6	This study
pSZ3-R109P	pACTrc /PomA+PotB Δ L1(Δ 46-82, R109P) -His_6	This study
pSZ4-R109P	pACTrc /PomA+PotB Δ L2(Δ 46-91, R109P) -His_6	This study
pSZ5-R109P	pACTrc /PomA+PotB Δ L3(Δ 41-82, R109P) -His_6	This study

Chapter 3:

Mechanism of stator activation in the native sodium-driven flagella

Introduction

Although we analyzed the chimeric Na^+-driven stator in *E. coli* cells, it does not completely represent the native Na^+-driven stator. Since the stator at the polar flagellum in *Vibrio alginolyticus* works functionally with the help of two unique ring structures, the T-ring and the H-ring (Terashima *et al.*, 2006; Terashima *et al.*, 2010). These extra structures are thought to reinforce the motor structure to resist the high revolution. Recent structural study demonstrated that FlgT acts as an assembly base or scaffold for both the ring structures (Terashima *et al.*, 2013). The T-ring is made up of MotX and MotY, and is located beneath the P ring, which is a part of bushing structure for the rod. The T-ring is an essential component to incorporate the stator unit into the motor (Terashima *et al.*, 2006). The periplasmic region of PomB is likely to bind to MotX (Okabe *et al.*, 2005), and MotX is connected to the basal body through the N-terminal domain of MotY (Kojima *et al.*, 2008b). Thus the stator unit of the sodium-driven motor is tightly fixed not only to the PG layer but also to the basal body through the interaction between PomB and T-ring.

In spite of the rigid anchoring structure, the stator unit of the sodium-driven motor still shows a dynamic behavior dependent on the binding of sodium ion to PomB (Fukuoka *et al.*, 2009). A recent deletion study of the periplasmic region of PomB ($PomB_C$) revealed that PEM of PomB is about 30 residues (121-153) longer in the N-terminal side than that of $MotB_C$ (Fig. 6) (Li *et al.*, 2011). This extra residues and the following residues before the conserved OmpA-like region show no clear sequence similarity to MotB (Fig. 6). To understand how does native Na^+-driven stator get activated, we

purified and crystallized various fragments of $PomB_C$ and solved the structure of $PomB_{C4}$ (121-315), which covers PEM of PomB, and $PomB_{C5}$ (135-315) (Fig. 14A). The crystal structures and following *in vivo* disulfide crosslink studies and motility assay revealed a novel insight into the molecular mechanism of the stator assembly and activation of the sodium driven flagellar motor.

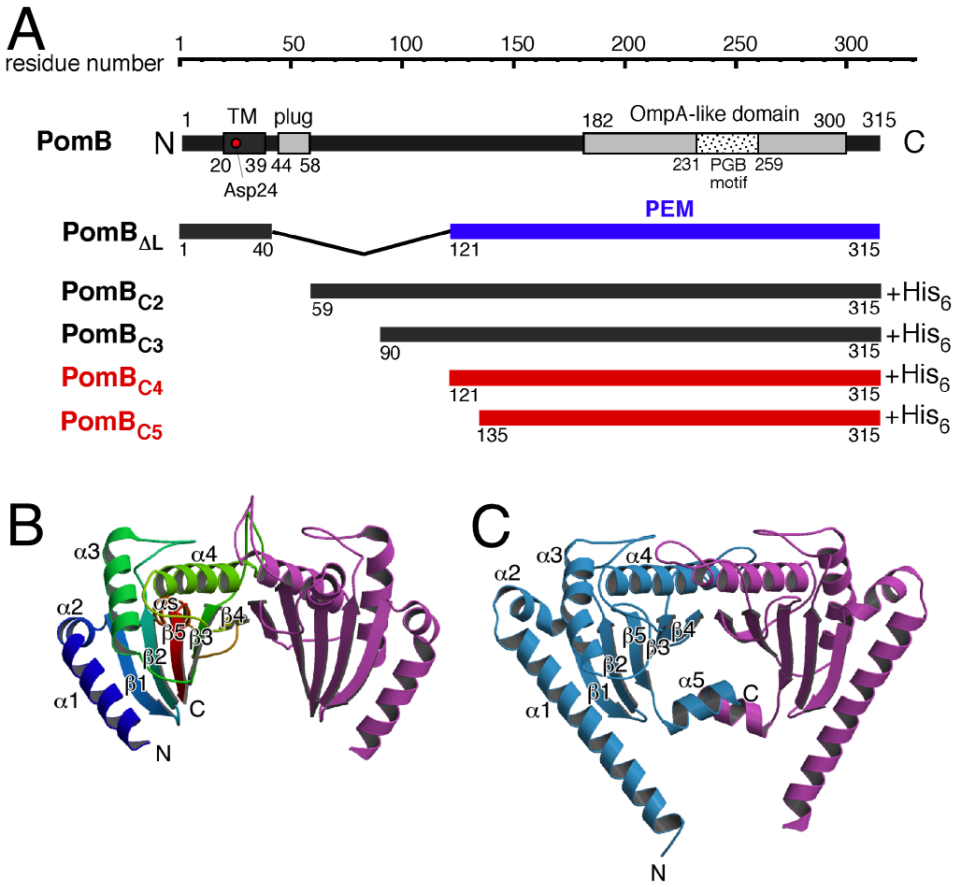

Fig. 14. Structure of the C-terminal fragment of PomB.

(A) Schematic representation of the full length PomB, PomB$_{\Delta L}$ and the PomB$_C$ variants used for crystallization. PomB$_{\Delta L}$ is the smallest fragment that forms a stable functional stator unit derived from a systematic deletion experiment (Li *et al.*, 2011). The PEM region is highligheted in blue. Asp-24, which is essential for ion translocation across the cytoplasmic membrane is shown in red circle. (B) Ribbon representation of PomB$_{C5}$ dimer. One subunit is color coded from blue to red from the N- terminus to the C-terminus, and the other is painted magenta. (C) Structure of *Salmonella* MotB$_{C2}$ dimer (PDB: 2ZVY) (Kojima *et al.*, 2009). The two subunits are colored in cyan and magenta.

Results

Structure of $PomB_C$

$PomB_{C4}$ and $PomB_{C5}$ were crystallized in the same space group of $P2_12_12_1$ with the almost same cell dimensions (Table 2). The two structures are basically identical, and the residues before 154 and after 305 are invisible in the density maps of both crystals. The structures of $PomB_{C4}$ and $PomB_{C5}$ were determined by 2.3 Å and 2.0 Å resolution, respectively. We therefore mainly describe the structure of $PomB_{C5}$ in this section. $PomB_C$ consists of a single OmpA-like domain composed of three α helices (α3, α4 and α5) and five β strands (β1, β2, β3, β4 and β5) with the N-terminal long and short α-helices (α1 and α2). Although the overall structure of $PomB_C$ shows remarkable similarity to that of *Salmonella* $MotB_C$ (St-$MotB_C$), marked differences are found in the N-terminal helices (α1 and α2), the loop connecting β3 and α4 (the β3-α4 loop), a short helix between β4 and β5 and the C-terminal region (Fig. 14B and 14C). The α1 helix of St-$MotB_C$ is projected from the core domain, whereas βinal $heli_C$ is ten residues shorter than that of St-$MotB_C$ and interacts with the core domain through its entire length. The orientation of nnecting β_C differs from that of St-$MotB_C$, and hence the angle formed by α1 and α2 is sharp in St-$MotB_C$ but obtuse in $PomB_C$. The conformation of the β3-α4 loop is quite different from St-$MotB_C$. This loop is thought to be included in the putative PG-binding site (Kojima *et al.*, 2009), because the corresponding loop of peptidoglycan-associated lipoprotein from *Haemophilus influenza* (Hi-Pal) interacts with the peptidoglycan precursor (Parsons *et al.*, 2006). The loop conformations of the five independent structures of St-$MotB_C$ are different each other, suggesting that the

loop is highly flexible (Kojima *et al.*, 2009). Thus the conformational difference of the loop of $PomB_C$ does not reflect the intrinsic property of $PomB_C$, but reflects the flexibility of this region. $PomB_C$ has a short helix between β4 and β5. This helix is not present in $MotB_C$ and MotY, but some other OmpA-like proteins, such as *Helicobacter pylori* $MotB_C$ (Hp-$MotB_C$) (Roujeinikova, 2008), Hi-Pal (Parsons *et al.*, 2006) and Pal from *E. coli* (Ec-Pal, PDB code: 1OAP) have it. The C-terminal residues following β5 are disordered in $PomB_C$. This region is folded into an α-helix in St-$MotB_C$, but deleting this helix has no effect on *Salmonella* motility (Muramoto and Macnab, 1998). Thus the structural difference of the C-terminal region is thought to be irrelevant to the stator function.

$PomB_C$ is known to form a dimer in solution (Li *et al.*, 2011). The asymmetric unit of the crystal contains a $PomB_C$ dimer, whose subunits are related by a pseudo two fold symmetry. The subunit arrangement of the dimer resembles that of the St-$MotB_C$ dimer. The subunit interface is formed by α4 and β4. The interaction between the two β4 strands creats an inter-subunit β-sheet and the side chain interactions between the two α4 helices stabilize the dimer (Fig. 15). These structure features are similar to St-$MotB_C$, however the residues involved in the subunit interaction are not conserved. Charged residues mainly contribute to the subunit interaction in St-$MotB_C$. On the contrary, hydrogen bonding network between hydrophilic neutral amino acid residues or between those and acidic or basic residues contribute to the subunit interaction in $PomB_C$ (Fig. 15). Moreover, other parts of the molecule, such as β3-α4 loop and α4-β4, are also involved in the interaction. Thus the dimeric structure $PomB_C$ seems more stable than

that of St-MotB$_C$.

Table 2. Data collection statistics

	PomB$_{C5}$ Native	PomB$_{C5}$ Os derivative	PomB$_{C4}$ Native
Space group	$P2_12_12_1$	$P2_12_12_1$	$P2_12_12_1$
Cell dimensions			
a, b, c (Å)	58.6, 63.3, 77.0	59.3, 64.6, 76.9	58.4, 63.3, 77.2
Wavelength (Å)	1.0000	1.1399	0.9741
Resolution (Å)	38.5-2.0 (2.11-2.0)	38.5-2.1 (2.21-2.1)	38.6-2.3 (2.42-2.3)
R_{merge}	9.9 (33.1)	7.1 (38.8)	9.9 (39.1)
I/σI	11.4 (4.7)	15.2 (4.3)	9.7 (3.7)
Completeness (%)	99.7 (100)	99.9 (99.9)	97.2 (97.2)
Anomalous (%)	-	99.9 (100)	-
Redundancy	7.2 (7.3)	7.1 (7.1)	4.6 (4.6)
Anomalous	-	3.6 (3.6)	-

Values in parentheses are for the highest resolution shell.

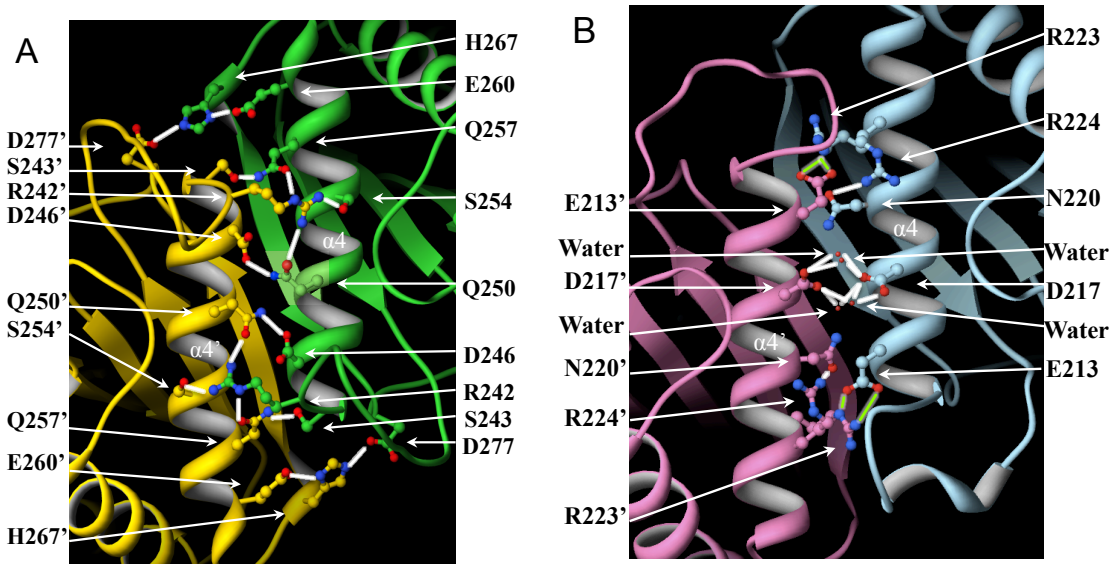

Fig. 15 Comparison of the dimer interface structure of $PomB_C$ and $MotB_C$.

Close up view of the interface of the $PomB_{C5}$ dimer (green and yellow) (A), and the $MotB_{C2}$ dimer (cyan and magenta, PDB: 2ZVY) (B). The residues involved in the side-chain interaction between the two subunits are labeled. Hydrogen bonds and electrostatic interactions are indicated by white and green bars, respectively.

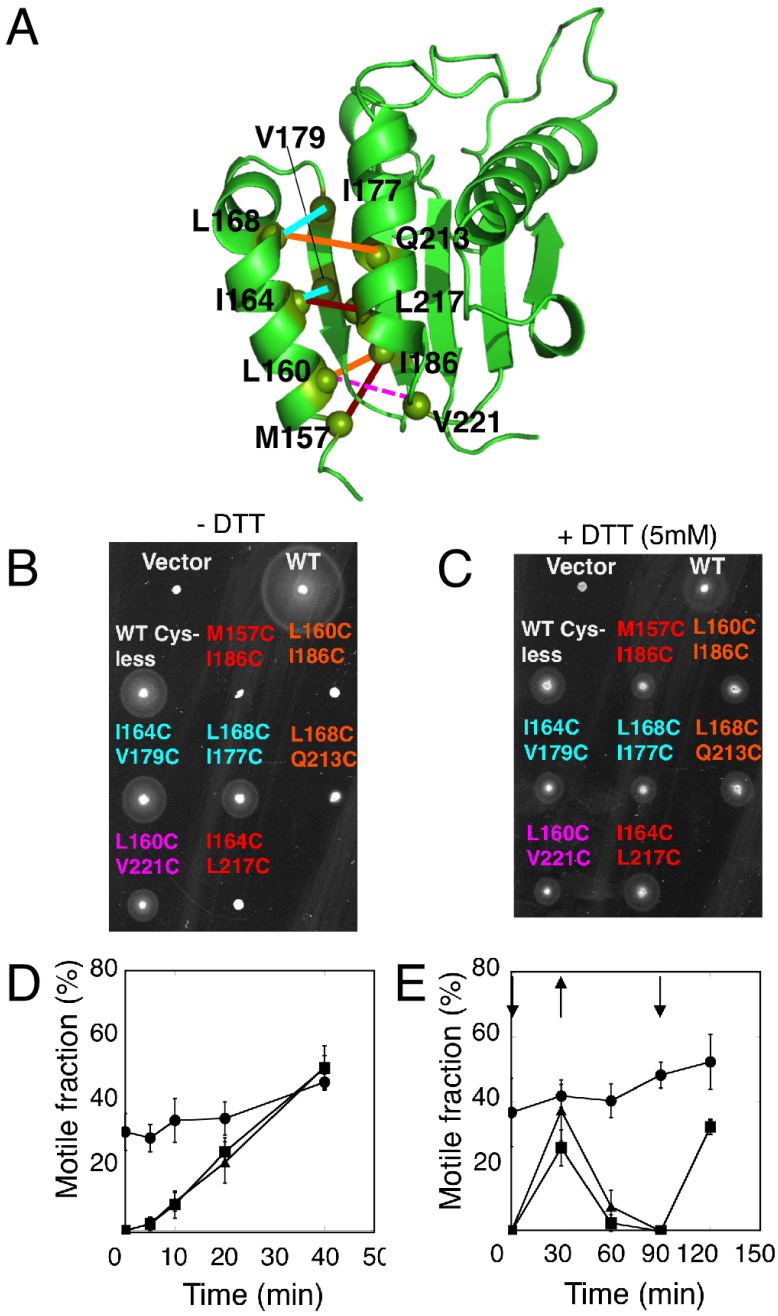

Fig. 16. Crosslink between α1 and core domain inhibits the function of stator

(A) Residues selected for cysteine substitution are mapped on the $PomB_C$ structure. Cα atoms of the selected cysteine substitution are indicated by ball on the ribbon diagram of $PomB_{C5}$. The residue pairs for double-cysteine substitution are shown by lines with color according to the motility and disulfide

crosslink formation: red lines, non-motile and crosslinked; orange lines, non-motile on soft agar plate but motile in liquid and crosslinked; blue lines, motile and crosslinked; the magenta broken line, motile and no-crosslink. (B) and (C) Motility of the double cysteine mutants of PomB. NMB191 (Δ*pomAB*) cells expressing mutant stator proteins from plasmids were incubated on the soft agar plate for 5.5 hours at 30 ºC in the absence of DTT (B) or in the presence of 5 mM DTT (C). The labels of the mutants are colored according to the motility phenotype and disulfide crosslink formation; magenta, motile and no-crosslink; blue, motile and crosslinked; orange, non-motile on soft agar plate but motile in liquid and crosslinked; red, non-motile and crosslinked. (D) Restoration of swimming motility in the presence of 1 mM DTT. DTT was added to the cell suspension at time 0 min. Wild type Cys-less PomB, PomB(M157C-I186C) and PomB(I164C-L217C) are shown in circle, triangle and square, respectively. (E) DTT dependent motility of the double cysteine mutants. Cell suspensions of Wild type Cys-less PomB (circle), PomB(M157C-I186C) (triangle), PomB(I164C-L217C) (square) were prepared and DTT was added to the final concentration of 1 mM to the suspensions at time 0 min. 30 min later, DTT was removed by washing with TMN medium without DTT. At time 90 min, DTT was added again to the suspension. Arrows at each time point represent DTT addition or removal.

Crosslinking between α1 and the core domain inhibits the motility

The structural similarity between $PomB_C$ and St-$MotB_C$ suggests that a conformational change of the N-terminal helical region of $PomB_C$ is required to anchor the stator unit. To detect the conformational change, we adopted an *in vivo* disulfide crosslinking approach. On the basis of the crystal structure of $PomB_C$, we selected seven pairs of residues that would be possible to form a disulfide bridge between α1 and the core domain when they were substituted to cysteine (Fig. 16A). To avoid interference of natural cysteine residues in PomB, we used a mutant PomB whose all three cysteine residues (Cys-8, Cys-10 and Cys-31) were replaced with alanine (Cys-less PomB) (Yorimitsu *et al.*, 2004) for the crosslinking experiments. This mutation slightly affects the motor function, but not drastically, compared to the wild type (Fig. 16B).

The *Vibrio* cells (Δ*pomAB*) transformed with plasmid pBAD33 encoding PomA and Cys-less PomB with the pair of cysteine substituion were inoculated onto the soft agar plates. The cells producing PomB(M157C-I186C), PomB(L160C-I186C), PomB(I164C-L217C) or PomB(I168C-L213C) did not show any motility for 5.5 h incubation (Fig. 2B). We observed a small and significant number of motile cells for PomB(L160C-I186C) and PomB(L168C-Q213C), respectively, but no motile cells for PomB(M157C-I186C) and PomB(I164C-L217C) in liquid under optical microscope (Table 3). These results suggest that the four double cysteine mutations influence the motor function, probably due to forming a disulfide bridge that may interfere the conformational change of the N-terminal helical region (Fig. 16A). The remaining three

mutants, PomB(I164C-V179C), PomB(L168C-I177C) and PomB(L160C-V221C), show comparable motility ring size to wild-type Cys-less PomB (WT Cys-less PomB) (Fig. 16B), indicating that these mutations did not affect the cell motility. Single cysteine substitutions of the residues that are selected for the double cysteine mutation experiments did not change the motility on the soft agar plate, suggesting that the cysteine replacement itself does not affect the stator function (Fig. 17A). We also confirmed that all the mutations did not change the expression level of the stator proteins in the host cell (Fig. 17B).

Table 3. Motile fraction for double Cysteine mutants.

Mutants	Motile fraction (%)
WT Cys-less	30.5
M157C-I186C	0
L160C-I186C	12.8
I164C-V179C	25.2
L168C-I177C	29.2
L168C-Q213C	29.2
L160C-V221C	32.8
I164C-L217C	0

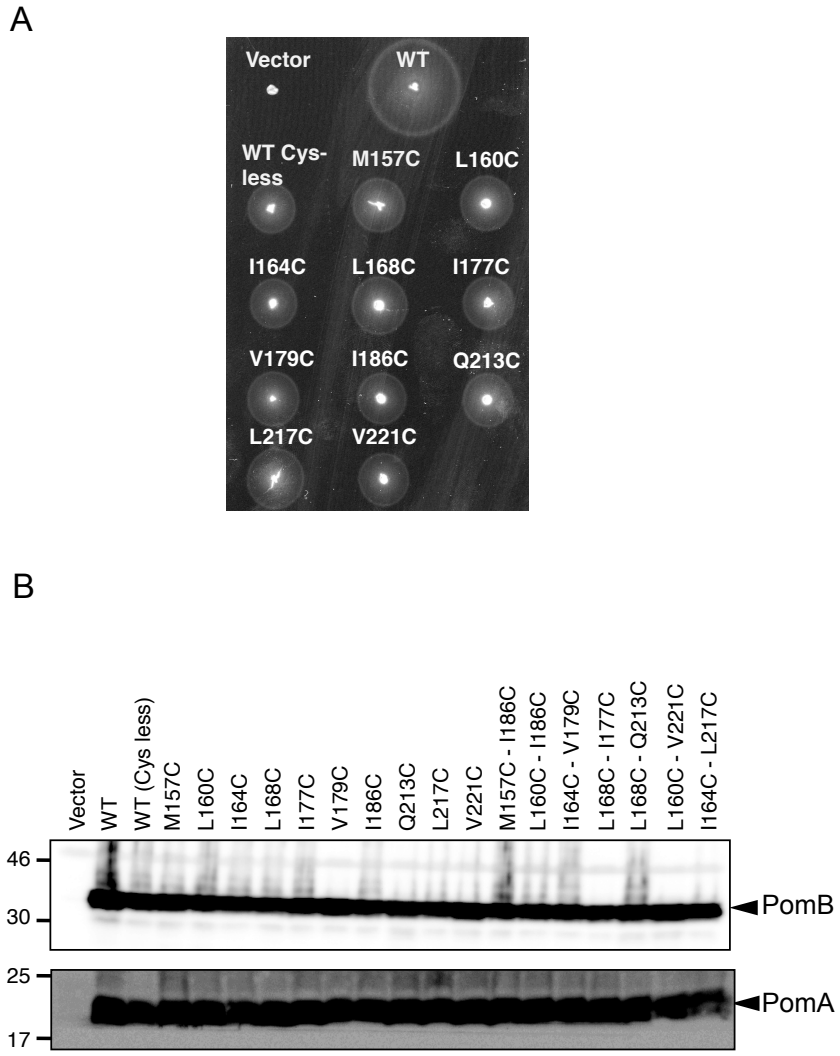

Fig. 17. Motility of the cells expressing mutant stators on the soft agar plates, and the cellular level of mutant PomB proteins.

(A) Motility of single cysteine mutants on the soft agar plate. NMB191 (Δ*pomAB*) cells expressing mutant stator protein were cultured on the soft agar plate containing 0.02% arabinose and 2.5 μg/ml chloramphenicol for 5.5 hours at 30°C. (B) Cellular level of PomA and mutant PomB. Whole cell lysates were separated by SDS-PAGE in the presence of β-mercaptoethanol, and detected by anti-$PomB_C$ antibody and anti-PomA1312 antibody.

Motility of the double cysteine mutants depends on reducing reagent

We found that the four double cysteine mutants lost motility on soft agar plate. If the motility is inhibited due to the disulfide bridge formation between cysteine pairs in the PomB, it would be restored by reduction of the disulfide bond. Then we added dithiothreitol (DTT), which is frequently used to reduce the disulfide bonds in proteins, into the soft-agar plate and observed motility of the cells. Addition of 5 mM DTT did not change the motility of the motile mutants and the WT Cys-less PomB. However, the non-motile mutants, PomB(M157C-I186C), PomB(I164C-L217C), PomB(L160C-I186C) and PomB(L168C-Q213C), showed motility rings almost the same size as the WT Cys-less PomB in the presence of 5 mM DTT (Fig. 16C). Although the wild-type cells with DTT showed a smaller motility ring than that without DTT, the motile fraction of WT cells was independent of the presence of DTT (Fig. 16C and Fig. 18B). These results suggest that the loss of motility of the mutants is due to the disulfide bridge formation between α1 and the core domain, and breakage of the disulfide bond by the reducing reagent restore the motility.

DTT dependent motility of the mutant cells is also detected in liquid. The cells were incubated in TMN buffer (50 mM Tris-HCl pH7.5, 5 mM Glucose, 5 mM $MgCl_2$ and 500 mM NaCl) with or without 1 mM DTT, and were observed under a dark-field optical microscope. The motile fractions of the cells producing PomB(M157C-I186C) or PomB(I164C-L217C) increased over time and reached to 50%, which is almost the same ratio as the WT Cys-less cells, after 40 min incubation with DTT (Fig. 16D). The swimming speed of the mutants also recovered more than 80% of the wild type after 30

min incubation (Fig. 18A). The DTT dependent restoration of motility was also observed for PomB(M157C-I186C) and PomB(I164C-L217C) cells treated with 1mg/ml kanamycin for 20 min, indicating that the motility recovery is not because of installation of newly synthesized stator proteins into the motor (Fig. 18C).

The recovered motility was lost again by removing DTT. The mutant cells after incubation in TMN buffer containing DTT for 30 min were harvested and moved into TMN buffer without DTT. The motile fraction was gradually reduced over time and the motility was completely lost after 60 min incubation. The motility was recovered by adding DTT again, so this DTT dependent motility is highly reproducible (Fig. 16E). On the contrary, the motile fraction of the WT Cys-less cells was not affected by the presence of DTT (Fig. 16E and 18B). These results support that the disulfide bridge formation between the α1 and the core domain of PomB inhibits the motility.

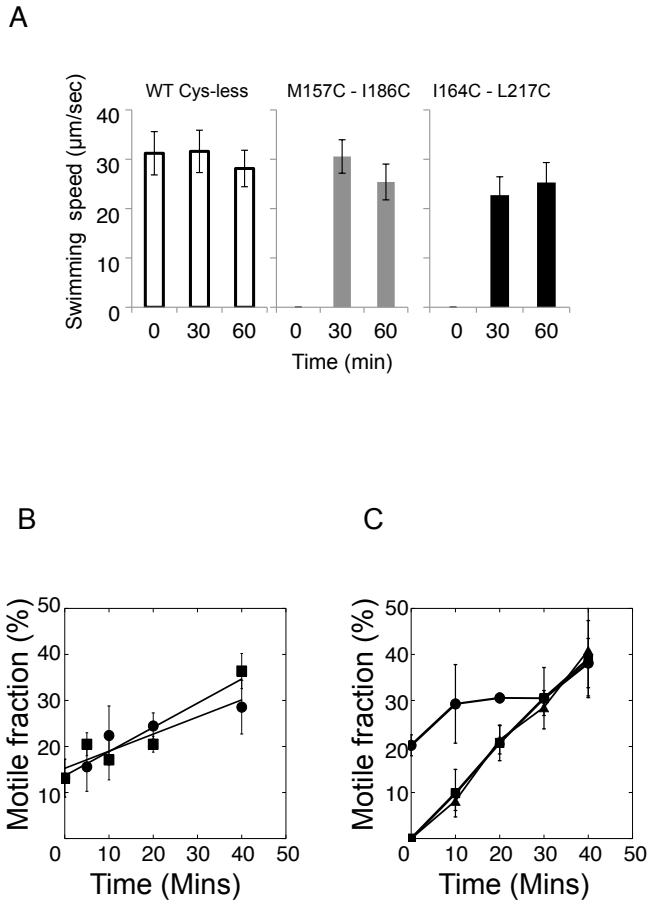

Fig. 18. Recovery of cell motility in liquid with an addition of DTT.

(A) Swimming speed of the Wild type Cys-less and double Cys mutant cells were measured at 0 minute, 30 minutes and 60 minutes after adding DTT (final concentration 1 mM). (B) Motile fraction of the Wild type Cys-less in the presence (square) or absence (circle) of DTT. Cell suspension was divided into two aliquots. DTT (final conentration 1 mM) was added to one aliquot at time zero, and nothing to the other. Each suspension was incubated at 30°C, and the number of swimming and non-swimming cells was counted at indicated time points. (C) Motile fraction in the presence of kanamycin and DTT. Cells were suspended in TMN buffer with 1 mg/ml kanamycin, and incubated at 30°C for 20 min to inhibit *de novo* protein synthesis. Then DTT (final concentration 1mM) was added at time 0. The cells were incubated at 30°C, and the number of swimming and non-swimming cells were counted at indicated time points. WT Cys-less, M157C-I186C and I164C-L217C are shown in circle, square and triangle, respectively.

Detection of disulfide bridge formation in the double cysteine mutants

To confirm the disulfide bridge formation in the PomB mutants, we detected free cysteine by modifying the thiol group with biotin maleimide. After incubation in buffer with 1mM DTT or without DTT for 35 min at 30 °C, the cells were treated with biotin maleimide and lysed. Then PomB was isolated from the solubilized cell membrane by immunoprecipitation with protein A conjugated beads and the anti-PomB antibodies. The amount of free cysteine in PomB was estimated by the level of the biotinylated PomB labeled with streptavidin-HRP. More free cysteine was detected when they were treated with DTT than without DTT for all the double cysteine mutants except for PomB(L160C-V221C), which shows similar strong bands both with and without DTT (Fig. 19A). Thus disulfide bridge is surely formed in the mutants except for PomB(L160C-V221C), and is reduced by addition of DTT. PomB(M157C-I186C), PomB(I164C-V179C), PomB(I164C-L217C) and PomB(L168C-I177C) indicated no or faint band without DTT, suggesting that disulfide bridge is fully formed in these mutants. We further confirmed the disulfide bridge formation of these four mutants by biotin-maleimide labeling in an *in vitro* method (Fig. 19B). It should be noted that a disulfide bridge is formed not only in the non-motile mutants but also in the motile mutants (Fig. 16B and 19B). On the contrary, PomB(L160C-I186C) and PomB(L168C-Q213C) show clear bands under without DTT condition (Fig. 3A), indicating a certain amounts of PomB were not crosslinked. This result is consistent with the fact that motile cells were observed in liquid for these mutants (Table 3).

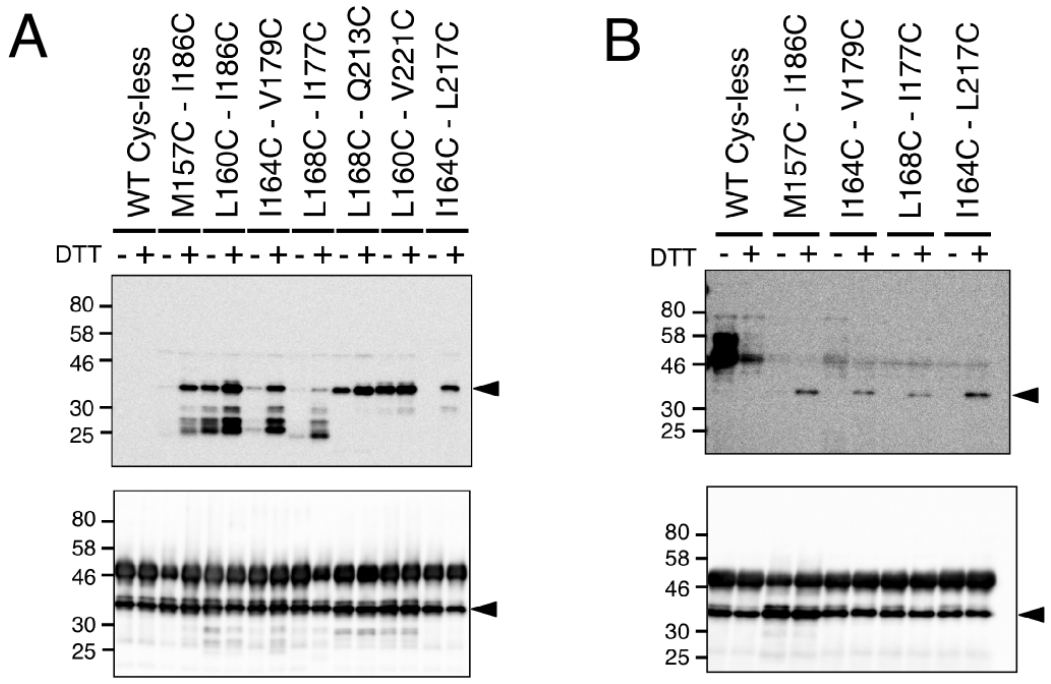

Fig. 19. Detection of the intramolecular disulfide bridge in PomB by thiol modification with biotin maleimide.

(A) *In vivo* labeling of PomB with free cysteine. PomB labeled with biotin maleimide was detected by streptavidin-HRP (upper panel), and total amount of PomB in the samples was detected by anti-$PomB_C$ antibody (lower panel). (B) *In vitro* labeling to confirm *in vivo* labeling results. PomB labeled with biotin maleimide (upper panel) and total amount of PomB in the samples (lower panel) were shown. The bands corresponding to PomB are indicated by arrow-heads.

The crosslinking does not affect the stator assembly around the rotor

The stator of *Vibrio* is known to assemble around the rotor in a sodium dependent manner (Fukuoka *et al.*, 2009). To assess the effect of disulfide crosslinking on the stator assembly around the rotor, we fused a GFP tag to the N-terminus of PomB(M157C-I186C), PomB(I164C-L217C) or WT Cys-less PomB, and observed the cells expressing each of the GFP-tagged PomB mutants by fluorescence microscopy. In the TMN buffer containing 500 mM NaCl, fluorescent dots were localized to the cell poles in both of the two mutants and the WT Cys-less cells, suggesting that the disulfide bridge formation of the PomB mutants does not affect the assembly of the stator (Fig. 20A and C). Without sodium ions (TMK buffer containing 500 mM KCl), however, the polar localization of stator is drastically decreased in all cells (Fig. 20B and C). These results indicate the dynamic assembly of the mutant stator is still dependent on sodium ion, having a same character to the wild type (Fukuoka *et al.*, 2009). Thus, we exclude the possibility that the loss of motility of the crosslinked mutants is caused by inhibition of the stator assembly around the rotor.

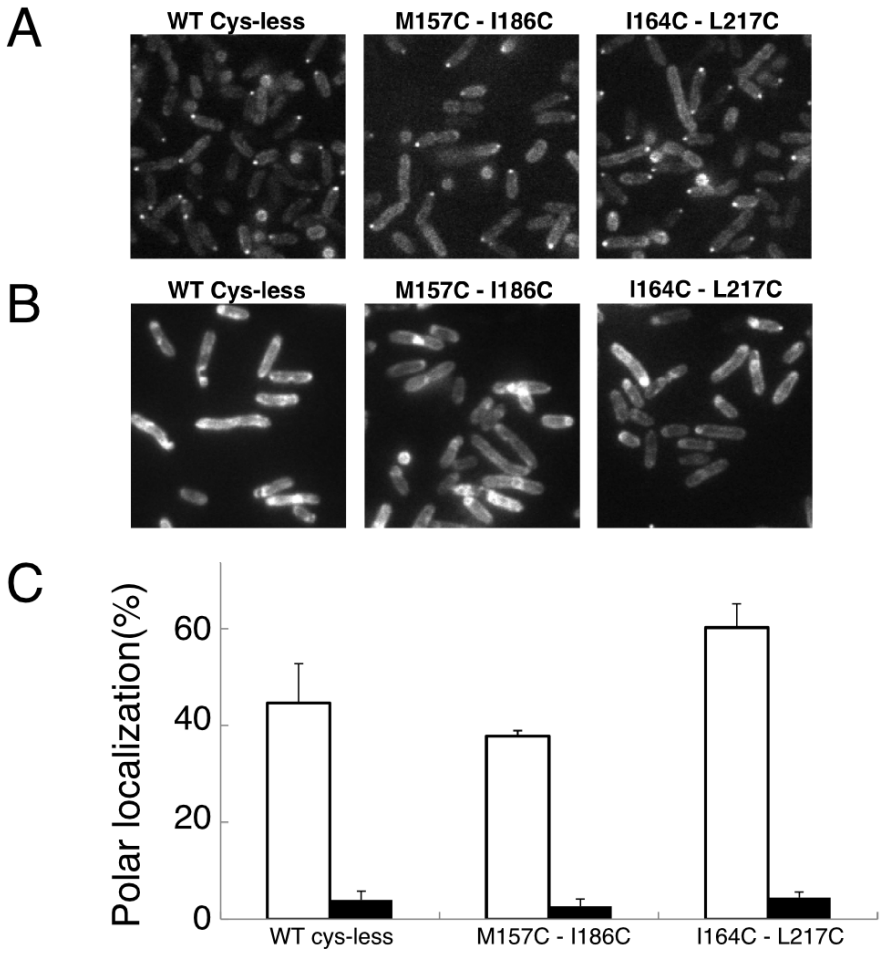

Fig. 20. Sodium dependent localization of the stator units with the PomB mutations.

(A) Representative fluorescent microscopic images of the GFP-fused stator complex in the presence of NaCl. The fluorescent foci at the cell pole indicate the assembly of the stator units around the rotor. (B) Representative fluorescent microscopic images of the GFP-fused stator complex in the absence of NaCl. (C) Polar localization of the stator was evaluated by counting the number of the cells with polar fluorescent foci in the observed field. Results in the presence or absence of NaCl were shown as open and closed bars, respectively.

The crosslinking does not inhibit the ion flow

Since the crosslinking did not affect stator assembly, we suspected that the crosslinking inhibits the ion conductivity of the stator channel. PomB/MotB has a periplasmic short segment called "plug" just at the C-terminal to their single trans-membrane region (Fig. 14A and Fig. 6). Overproduction of the mutant stator complex without the segment caused severe growth impairment (Hosking *et al.*, 2006). We previously showed that overproduction of the plug-deleted PomA/PomB complex inhibits cell growth (Li *et al.*, 2011), and this effect was more severely observed in *E. coli* than in *Vibrio* (Takekawa *et al.*, 2013). We also showed that growth inhibition was correlated with the massive influx of sodium ion through the overproduced mutant stators (Takekawa *et al.*, 2013), thus we can evaluate the ion-conducting activity of the stator by this simple assay. To analyze the crosslinking effect on the ion conductivity, we performed the growth assay of *E. coli* cells expressing PomA and PomB mutants. When PomB that lacks the plug region (Δ41-60 of PomB) was over-expressed with PomA, cells showed strong growth inhibition, regardless of the presence of additional M157C-I186C mutation (Fig. 21). This suggests that the crosslink at position 157 and 186 of PomB did not disturb the ion-conductivity of the stator.

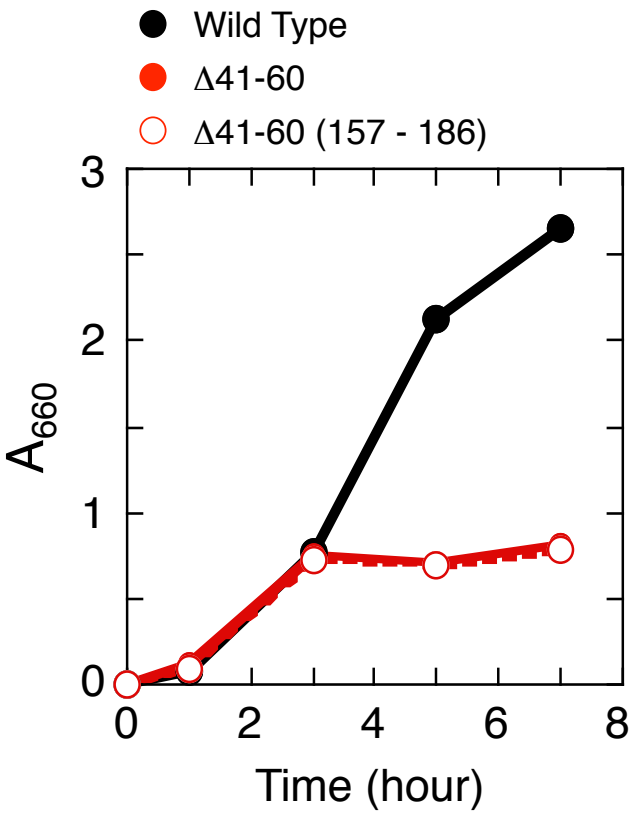

Fig. 21. Growth of *E. coli* DH5α cells expressing wild-type or mutant PomB with PomA

The black line and solid circles represent wild-type; the red line and solid circles represent the plug deletion mutant of PomB; the red broken line and open circles represent the plug deletion with the 157-186 double cysteine substitution. At each time point, cell growth was monitored by measuring the absorbance at 660 nm.

Discussion

The *Vibrio* sodium-driven motor rotates around 100,000 rpm, which is five times faster than the *Salmonella* or *E. coli* proton driven motor. To stand such rapid rotation, the sodium-driven motor has extra ring structures, the T-ring and the H-ring, in the periplasmic space. The stator units assemble around the rotor with proper orientation through the interaction between the T-ring and the C-terminal periplasmic region of PomB (Okabe *et al.*, 2005; Terashima *et al.*, 2006; Kojima *et al.*, 2008b). Thus $PomB_C$ is expected to have a specific structure for the interaction with the T-ring. The overall structure of $PomB_C$ is similar to that of St-$MotB_C$ and no such extra structure was found. The electrostatic surface potential indicates that the N-terminal helical region of $PomB_C$ is negatively charged, whereas St-$MotB_C$ has no special charge distribution on its corresponding region (Fig. 22A and 22B). We therefore substituted the negatively charged residues of α1 and α2 to positively charged residues (E156K, E158K, E162K, E169K and E173K) (Fig. 22C). These substitutions, however, did not affect motility of the mutant cells even when all the five residues were replaced at a time (Fig. 22D). Then where is the interaction site of PomB for the T-ring? The most plausible candidate is the N-terminal disordered region of $PomB_{C4}$, which corresponds to PEM of PomB (Li *et al.*, 2011). The N-terminal side of PEM in the PomB is about 30 residues (121-153) longer than that of $MotB_C$. These residues show no similarity with MotB in the sequence (Fig. 6) and are indispensable for *Vibrio* motility. Thus it is possible that the N-terminal disordered region is responsible for an interaction with the T-ring.

The dimer structure of $PomB_C$ seems to be more stable than that of St-$MotB_C$. The

many hydrophilic interactions on the dimer interface strengthen the $PomB_C$ dimer. The *Vibrio* polar flagellar motor rotates five times faster than the *Salmonella* motor. The interactions are probably needed to resist the quick revolution of the *Vibrio* motor.

In a previous study, it was solved that the structure of St-$MotB_C$ that fully covers PEM and suggested that a large conformational change of the N-terminal region of PEM is required for anchoring the stator to the peptidoglycan layer and stator activation (Kojima *et al.*, 2009). Here we solved the crystal structure of $PomB_C$ and the structure is similar to that of St-$MotB_C$, suggesting that the *Vibrio* PomA/B stator shares the common activation mechanism to the *Salmonella* MotA/B stator. This fact led us to test the conformational change by using intramolecular crosslinking approach. Among seven pairs of double Cys replacements in $PomB_C$ (one in the α1 helix and the other in the core domain), four pairs (M157C-I186C, L160C-I186C, I164C-L217C, and I168C-Q213C) lost motility on soft agar plate (Fig. 16B), and the motility was restored by adding DTT (Fig. 16C). Such a reversible inhibition of motility supports our conformational change model. However assay of free cysteine residues revealed that the motile mutants (I164C-V179C and L168C-I177C) also form a disulfide bridge (Fig. 19). This result seems to be inconsistent with the model, thus careful interpretation is necessary for the mutation experiments.

The PomB(M157C-I186C) and PomB(I164C-L217C) mutant cells completely lost motility and the disulfide bridge was almost perfectly formed. On the contrary, the PomB(I164C-V179C) and the PomB(L168C-I177C) mutant cells showed normal motility, in spite of the disulfide bridge being almost completely formed. The

PomB(L160C-I186C) mutant and PomB(L168C-Q213C) mutant did not show motility on soft agar plate, but a lot of cells were motile in liquid. The disulfide formation assay revealed that the PomB(L160C-I186C) mutant and PomB(L168C-Q213C) mutant are partially crosslinked. This type of behavior is often seen in chemotactic mutants or flagellar switching mutants. Thus the disulfide bridge in both mutants probably caused a defect not in torque generation but in the rotational switching of the motor. Furthermore the motility of these two mutants on soft agar plate was fully recovered by an addition of DTT (Fig. 16C). Thus, only the non-crosslinked cells were thought to be motile. The PomB(L160C-V221C) mutant cells show normal swimming behavior. This is consistent to the fact that no crosslink was observed for the PomB(L160C-V221C) mutant. Taking these results together, intramolecular crosslink at 157 or 160 inhibits the motility, but that at 168 does not. This suggests that the N-terminal two-thirds of α1 changes its conformation to activate the motor but the C-terminal one-third of α1 remains as a helix structure. Crosslink at 164 gave contradictory results on molity depending on the disulfide crosslinking partner. The I164C-V179C mutant is motile, whereas the (I164C-L217C) mutant is not. Leu-217 is in α3, which interacts to the N-terminal region of α1. The disulfide formation stabilizes the interaction between α1 and α3, resulted in hindering the conformational change of the N-terminal region of α1. On the contrary, Val-179 is in β1 and has an interaction to the C-terminal region of α1 but no interaction to the N-terminal region. Thus disulfide formation does not affect the N-terminal conformational change of α1.

To fix the stator to the PG layer, an N-terminal large conformational change is

expected for the periplasmic domain of the stator B subunit. Our disulfide crosslinking experiments of PomB suggest that the N-terminal two thirds of α1 (154-164) changes its conformation. However, if this region (11 residues) adopts a fully extended conformation, it becomes longer only about 22 Å, which seems insufficient to reach the PG layer. PEM of PomB begins from Asp-121 and the N-terminal region of PEM (121-153) is disordered in the crystal structure of $PomB_{C4}$. Thus, it is possible to form a structure to reach the PG layer with the disordered region, even though some of the region may be needed for interaction to the T-ring.

St-MotB (Δ51-100), a deletion mutant of St-MotB is known to form a stable motor (Muramoto and Macnab, 1998). If St-MotB adopts the similar structural change as PomB, the residues of α1 before Leu-123 which corresponds to Ile-164 in PomB, change their conformation. If they adopt fully extended conformation, it becomes about 77 Å, which is enough size to reach the PG layer considering the size of the St-$MotB_C$ domain. Since the St-MotB mutant lacking 51-110 still can swim though the motor is unstable (Muramoto and Macnab, 1998), PEM of St-MotB is defined starting from Met-111, which corresponds to Glu-152 in PomB. If the conformational transition occurs in the same corresponding region of PomB (M111-L123 of MotB), gain of the length is only about 26 Å. Thus, structural change of the whole α1 helix may be required to reach the PG layer for MotB.

On the basis of this study together with the previous results, we propose a model for activation mechanism of the *Vibrio* sodium-driven motor (Fig. 23). The stator diffusing in the cell membrane is in an inactive state before incorporating into the motor (i).

When the stator reaches around the rotor, PomA interacts with FliG (ii). This interaction triggers opening of "plug" (iii) that allows sodium ion to translocate into the channel of the stator complex. The sodium flow may induce the binding of PomB to the T-ring. This step probably includes a conformational change of the disordered N-terminal region of PEM (iv). After that, the N-terminal two thirds of α1 changes its conformation to an extended form to anchor to the PG layer (v). Localization of the stator is dependent on sodium and no stator localization was observed in the PomB D24N mutant (Fukuoka *et al.*, 2009), suggesting that the stator localization requires sodium binding to Asp-24, which is in the trans-membrane helix of PomB. Thus the plug opening should occur in the early stage of the stator assembly process. The binding of PomB to the T-ring may follow or coincide with this event to anchor the stator unit around the rotor. Without binding to the T-ring, the stator unit is not stably anchored and easy to disassemble from the motor (Terashima *et al.*, 2006). If the binding of PomB to the T-ring occurs first, localization of the stator would have not been observed dynamic assembly of the stator dependent on sodium ions. Moreover, we suggest that the conformational change of α1 is the final step of the stator assembly process because the stator M157C-I186C shows polar localization around the rotor and ion-conductivity. With this conformational change, the stator unit would be firmly fixed to the PG layer with proper orientation allowing the rotation of the motor. However, how does sodium ion triggers the assembly of the stator unit and how are the conformational changes induced are awaiting to be solved.

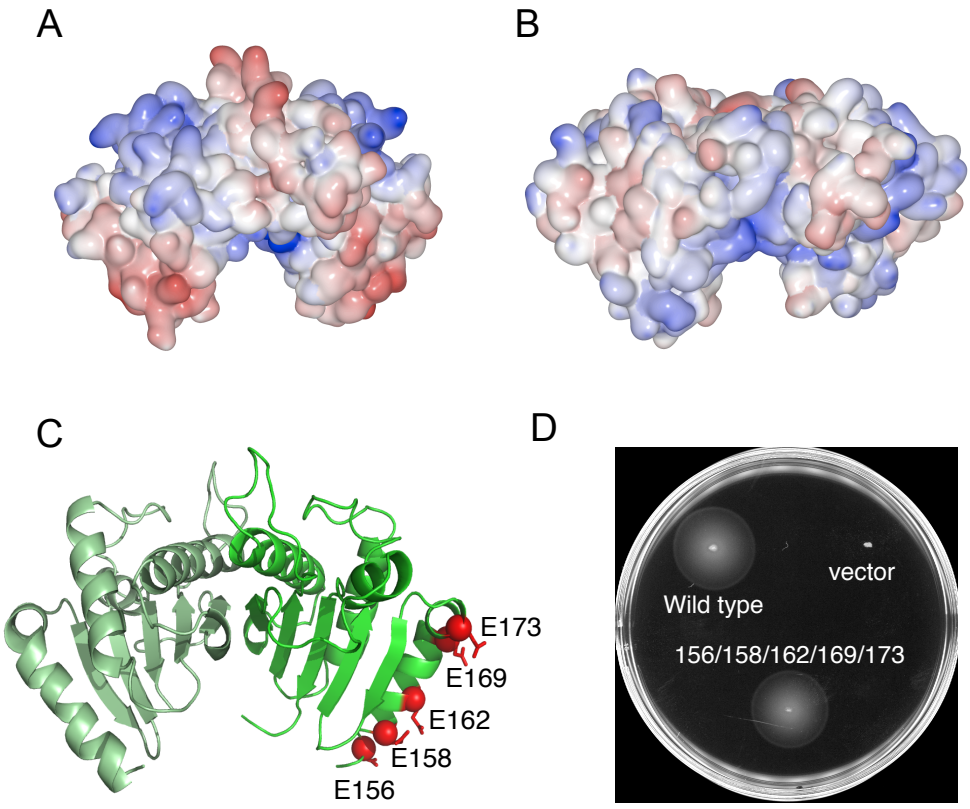

Fig. 22. Mutation of the negatively charged residues of the N-terminal region of $PomB_C$. Electrostatic surface potential distribution of the $PomB_{C5}$ dimer (A) and the $MotB_{C2}$ dimer (B). (C) The N-terminal negatively charged residues that contribute to the exposed surface potential of $PomB_C$ (E156, E158, E162, E169 and E173) are mapped on the ribbon diagram of $PomB_C$. The side chain and the C α atom of the residues are indicated by red stick and red ball, respectively. (D) Motility of the charge-reversed mutant on the soft agar plate. Fresh single colony of the strain NMB191 (Δ*pomAB*) that harbors plasmid pHFAB (for mutant or wild-type *pomAB* expression) or pBAD33 (vector) was inoculated on the 0.3% agar VPG plate containing 0.02% arabinose and incubated at 30°C for 8 hours. We replaced all five negatively charged residues to positively charged lysine (156/158/162/169/173), but this mutant did not show any defect in motility.

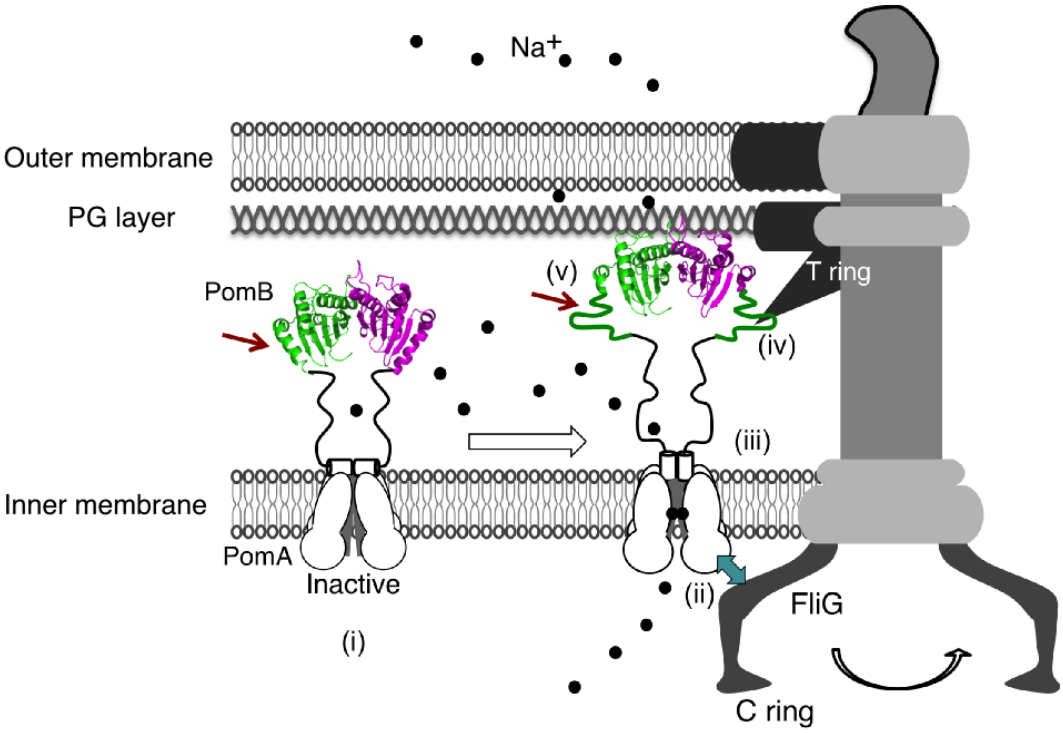

Fig. 23. A plausible model for the assembly of the Na^+-driven stator.

(i) The stator diffusing in the cell membrane. When the stator reaches around the rotor, PomA interacts with FliG (ii). This interaction triggers opening of "plug", which is shown by two small cylinders (iii). Then the conformational change of the disordered N-terminal region of PEM (bold lines) occurs to bind to the T-ring (iv), followed by the conformational change of the N-terminal two thirds of α1 (shown by the brown arrow) to reach the core domain to the PG layer (v).

Material and Method

Bacterial strains, plasmids and mutagenesis

Bacterial strains and plasmids used in this study are listed in Table 4. Point mutations were generated using QuikChange site-directed mutagenesis protocol (Stratagene). The plasmid pHFAB (encoding for the *pomA* and *pomB* gene) was used as the template. Plasmids were isolated from *E. coli* DH5α by Promega SV Minipreps Kit (Promega) and QIAprep Spin Miniprep Kit (Qiagen) and introduced into the *Vibrio* cell by electroporation with parameters of 1.4 kV and 200Ω (Kawagishi *et al.*, 1994). The stator proteins including mutants were expressed under the control of the arabinose-inducible *araBAD* promoter. All the plasmids carry the chloramphenicol resistance. Mutations were confirmed by using the ABI Prism 3130 genetic analyzer (Applied Biosystems).

Protein preparation and crystallization

C-terminally His6-tagged $PomB_{C4}$ (residues 121-315 of PomB) and $PomB_{C5}$ (residues 135-315 of PomB) were overproduced in *E. coli* BL21(DE3) from the plasmid pTSK35 ($PomB_{C4}$) and pTSK36 ($PomB_{C5}$), and purified as described previously (Li *et al.*, 2011) with slight modification. Shortly, after the HisTrap column (GE healthcare) purification, peak fractions of $PomB_{C5}$ were pooled and concentrated by ultrafiltration using an Amicon Ultra device (Millipore). Then 10 times volume of buffer B (20 mM Tris-HCl pH8.0, 100 mM NaCl) was added, and concentrated again by ultrafiltration to exchange the buffer content. $PomB_{C4}$ was further purified after the HisTrap column treatment

using a HiTrapQ column (GE healthcare) with a linear gradient of 10-1000 mM NaCl in buffer A (20 mM Tris-HCl pH8.0, 10 mM NaCl). The peak fractions were pooled and concentrated as did for $PomB_{C5}$. Final concentrations of purified protein used for crystallization were 19.4 mg/ml for $PomB_{C4}$ and 33 mg/ml for $PomB_{C5}$.

Crystal screening was performed by the sitting-drop vapour-diffusion technique with commercially available screening kits Wizard I and II (Emerald BioSystems) and Crystal Screen I and II (Hampton Research) at 293 K. Each drop was prepared by mixing 0.2 ml of protein solution with 0.2 ml of reservoir solution, and equilibrated to 100 ml of reservoir solution. $PomB_{C4}$ crystals were grown from drops containing 20% (w/v) PEGMME2000, 0.1 M imidazole pH6.5 and 4% (v/v) MPD. Rectangular crystals appeared overnight and grew to typical dimensions of 0.1 x 0.03 x 0.02 mm within 2-3 days. The space group of the crystals was orthorhombic $P2_12_12_1$ with unit cell dimensions a = 58.4, b = 63.3, and c = 77.2 Å. $PomB_{C5}$ crystals were grown from drops containing 16% (w/v) PEGMME2000, 0.1 M acetate pH6.0 and 5% (v/v) MPD at 293 K. Pyramid-like crystals appeared overnight and grew to typical dimensions of 0.06 x 0.06 x 0.03 mm within 2-3 days. The space group of the crystals was $P2_12_12_1$ with unit cell dimensions a = 59.3, b = 64.6, and c = 76.9 Å. Osmium derivative crystals were prepared by soaking the crystals in a reservoir solution containing K_2OsCl_6 at 50% saturation for 12 hours.

Data collection and structural determination

Diffraction data were collected at beamlines BL32XU and BL41XU in SPring-8

(Harima, Japan) with the approval of the Japan Synchrotron Radiation Research Institute (JASRI) (Proposal No. 2010B1901 and 2011A1240). Crystals were soaked in a cryo-protectant solution containing 10% (v/v) MPD and 90% (v/v) of the reservoir solution for several seconds, and then were transferred into liquid nitrogen for freezing. The X-ray diffraction data were collected under nitrogen gas flow at 100 K. The statistics of the diffraction data are summarized in Table 2. The diffraction data were processed with MOSFLM (Leslie, 1992) and were scaled with SCALA (Winn *et al.*, 2011). The initial experimental phase of $PomB_{C5}$ was calculated using the SAD data of the Os derivative with a program Phenix (Adams *et al.*, 2002). The atomic model of $PomB_{C5}$ was constructed with Coot (Emsley and Cowtan, 2004) and refined against the native data to 2.0 Å with Phenix (Adams *et al.*, 2002). The refinement R factor and the free R factor were converged to 18.7% and 23.8%, respectively. The Ramachandran plot indicated that 89.4% and 10.6% residues were located in the most favorable and allowed region, respectively. The structure of $PomB_{C4}$ was determined by molecular replacement with Phenix (Adams *et al.*, 2002) using the atomic model of $PomB_{C5}$ as a search model. The model was modified with Coot (Emsley and Cowtan, 2004) and refined to 2.3 Å with Phenix (Adams *et al.*, 2002). The final refinement R factor and the free R factor were 17.5% and 23.4%, respectively. The Ramachandran plot indicated that 93.6% and 6.4% residues were located in the most favorable and allowed region, respectively. Structural refinement statistics are summarized in Table 5.

Motility assay

Vibrio alginolyticus strains harboring vectors or plasmids were cultured overnight at 30ºC on VC medium (0.5% Polypeptone, 0.5% Yeast Extract, 3% NaCl, 0.4% K_2HPO_4, 0.2% glucose) including 2.5 μg/ml chloramphenicol. 2 μl of overnight cultures were inoculated on the surface of VPG soft agar plates (1% Bacto Tryptone, 3% NaCl, 0.3% agar, 0.4% K_2HPO_4, 0.5% Glycerol) including 2.5 μg/ml chloramphenicol and 0.02% arabinose, with or without 5 mM DTT. The plates were incubated at 30ºC for 5.5 hours to observe motility rings. Cells for the swimming measurement were grown in VPG medium containing 2.5 μg/ml chloramphenicol and 0.02% arabinose until late-log phase (typically 4 hours) at 30°C, harvested and washed once and resuspended by TMN buffer (50 mM Tris-HCl pH7.5, 5 mM Glucose, 5 mM MgCl and 500 mM NaCl) (Yorimitsu, 2000). This suspension was incubated at 30°C for 10 min to equilibrate cells to the buffer condition, and then DTT was added to the final concentration of 1 mM at time 0. At each time point, 5 ml of suspension was taken and diluted 100 times with the fresh TMN buffer, followed by immediate observation of motility under a dark-field microscope. To avoid the change of direction for the swimming, 10 mM serine was included in the buffer. During the measurement, the cell suspension were kept at 30°C. Motile fraction of the cells was determined as described (Kojima *et al.*, 2011), and swimming speed of the cells was analyzed as described (Zhu *et al.*, 2012). DTT was removed from the cell suspension (for Fig. 16E) by washing cells twice with TMN buffer.

Detection of proteins from whole cell lysate

Cells were cultured until they reached log phase of growth in VPG medium containing 0.02% arabinose and 2.5 μg/ml chloramphenicol. Cells were harvested and suspended to the SDS-PAGE loading buffer (66 mM Tris-HCl pH6.8, 8.3%(w/v) glycerol, 1% SDS, 16%(v/v) b-mercaptoethanol, 0.003% Bromophenol Blue) at a cell concentration equivalent to an OD_{660} of 10. After boiling the mixture at 95°C for 5 min, proteins were separated by SDS-PAGE and immunoblotting was carried out as previously described using an anti-PomA1312 antibody (Yorimitsu *et al.*, 1999) or an anti-$PomB_C$ antibody (Terauchi *et al.*, 2011).

Detection of disulfide formation

For the crosslinking study, we selected four residues (Met-157, Leu-160, Ile-164 and Leu-168) that are present in α1 and face to the core domain of $PomB_C$. We measured the distance between the C_β atoms of the selected residues and their neighboring residues, and picked up the closest and the second closest neighboring residues for crosslinking candidates. Although the second closest neighbor of Leu-168 is Val-179, we did not select it because Val-179 is located on the same β-strand as Ile-177, which is the closest residue of Leu-168. Instead, the third closest residue, Gln-213, was chosen. The second closest neighbor of Met-157 is Gln-302, but it was not selected because it locates at the C-terminus of the visible region of $PomB_C$. As a result, the seven residue pairs (M157-I186, L160-I186, L160-V221, I164-V179, I164-L217, L168-I177 and L168-Q213) were chosen for the targets of the double cysteine substitution. The mutant cells were harvested after 4 hours culture in VPG medium containing 0.02% arabinose

and 2.5 μg/ml chloramphenicol, suspended in TMN buffer with DTT (1 mM) or without DTT, and incubated for 40 min at 30°C. The cells were collected by centrifugation and resuspended in the TMN buffer. To detect free cysteine in PomB in the cell, biotin maleimide was added to the suspension to the final concentration of 4 mM, and incubated at 30ºC for 10 min. Then the cells were washed twice by TMN and disrupted by sonication. The unbroken cells were removed by centrifugation, and the cell lysate was subjected to ultracentrifugation (112,000 x *g* for 30 min at 4ºC). The pellet (membrane fraction) was dissolved in TNET buffer (50 mM Tris-HCl pH8.0, 150 mM NaCl, 5 mM EDTA and 1% Triton X-100) and incubated on ice for 30 min. After removing the insoluble materials by centrifugation (16,100 x *g*, for 10 min), 5mg of Protein-A sepharose CL-4B beads (GE Healthcare) equilibrated with TNET buffer was added to the supernatant and the solution was incubated for 30 min at 4°C to avoid non-specific binding of beads. After flash centrifugation to remove beads, new Protein-A sepharose beads and anti-PomB antibody was added to the supernatant and the mixture was incubated overnight with gentle rotary mixing. Then the beads were washed with TNET buffer for three times, and the bound proteins were eluted from the beads by boiling the beads in SDS-PAGE loading buffer for 5 min. Protein samples were separated by SDS-PAGE, transferred onto the PVDF membrane and biotinylated PomB was detected with streptoavidin-conjugated horseradish peroxidase (GE Healthcare) and chemiluminescence. Total amount of PomB in the immunoprecipitates was detected by anti-$PomB_{C2}$ antibody.

Free cysteine in PomB was also detected by *in vitro* labeling of thiol groups with

biotin maleimide. Cells expressing mutant or wild-type stator were grown in VPG, harvested as described above for the *in vivo* labeling experiment. Cells were suspended to 500 ml of TMN buffer at a cell concentration equivalent to OD_{660} of 5. The cells were divided into two groups; one was incubated with 1mM DTT, and the other without DTT at 30°C for 40 minutes. After the motility of each strain was observed under the dark-field microscope, the cell suspension of 100 μl were mixed with 100 μl of 2% SDS, and were boiled at 95°C for 10 minutes followed by cooling them down to room temperature. Then biotin-maleimide was added to the final concentration of 2 mM, and the mixture was further incubated at 37°C for 30 minutes. The reaction was stopped by adding cysteine to the final concentration of 4 mM (Narita *et al.*, 2013). PomB was immunoprecipitated, and biotin-labeled PomB was detected with streptavidin-conjugated horseradish peroxidase as described above.

Observation of the subcellular localization of GFP-PomB

Localization of the stator was observed as described previously (Kojima *et al.*, 2011). In brief, NMB191 cells harboring the plasmid pHFGBA2 were cultured overnight in VC medium, then the culture were diluted 100-fold in VPG medium containing 0.006% arabinose and 2.5 mg/ml chloramphenicol. Cells were cultured for 4 hours at 30°C, then were harvested and resuspended in TMN buffer (50 mM Tris-HCl pH 7.5, 5 mM $MgCl_2$, 5 mM glucose, 500 mM NaCl), or TMK buffer (50 mM Tris-HCl pH 7.5, 5 mM $MgCl_2$, 5 mM glucose, 500 mM KCl). The resuspended cells were fixed with 0.1% (w/v) Poly-L-lysine and were observed by fluorescence microscopy (Olympus, BX50).

Monitoring cell growth

Cell growth was monitored as described previously with slight modification (Zhu *et al.*, 2012). *E. coli* DH5a cells harboring plasmids were cultured overnight at 37°C in LB medium containing 25 mg/ml chloramphenicol. The overnight cultures were diluted 100-fold in 3 ml LB medium containing 25 mg/ml chloramphenicol and 0.02% (w/v) arabinose, and were further cultured for 7 hours at 37°C with shaking. Cell densities were monitored at an optical density of 660 nm (OD_{660}) at indicated time points (0, 1, 3, 5, 7 hours). Growth curves were measured at least twice, and representative results were shown in the figures (Fig. 21).

Table 4. Bacterial strains and plasmids

Strain or plasmid	Geotype or desecription	Source
***V. alginolyticus* strains**		
VIO5	VIK4 *laf* (Rif^{r} Pof^{+} Laf^{-})	(Okunishi *et al.*, 1996)
NMB191	VIO5 Δ*pomAB*	(Yorimitsu *et al.*, 1999)
***E. coli* strains**		
BL21(DE3)	Recipient for protein overproduction	
DH5 α	Recipient for cloning experiments	
Plasmids		
pET19b	T7 expression vector	Novagen
pTSK33	pET19b/PomB$_{C2}$-His$_6$	(Li *et al.*, 2011)
pTSK34	pET19b/PomB$_{C3}$-His$_6$	(Li *et al.*, 2011)
pTSK35	pET19b/PomB$_{C4}$-His$_6$	(Li *et al.*, 2011)
pTSK36	pET19b/PomB$_{C5}$-His$_6$	(Li *et al.*, 2011)
pBAD33	*pBAD* promoter, Cm^{r}	(Guzman *et al.*, 1995)
pHFAB	pBAD33/PomA+PomB	(Fukuoka *et al.*, 2009)
pHFAB Cys-less	pHFAB(C8A,C10A and C31A)	H.Terashima
pHFGBA2	pBAD33/GFP+PomB+PomA	(Fukuoka *et al.*, 2009)
pLSK9	pBAD33(PomA+PomB$_{\Delta L}$(Δ41-60))	(Li *et al.*, 2011))

Table 5. X-ray refinement statistics

	$PomB_{C5}$	$PomB_{C4}$
Resolution range (Å)	37.6-2.0 (2.05-2.0)	33.0-2.3 (2.39-2.3)
No. of reflections working	19,880 (1,258)	12,759 (1,286)
No. of reflections test	1,979 (140)	1283 (142)
R_w (%)	18.7 (20.8)	17.5 (20.9)
R_{free} (%)	23.8 (30.2)	23.4 (27.6)
Rms deviation bond length (Å)	0.007	0.006
Rms deviation Bond angle (°)	1.06	1.01
B-factors		
Protein atoms	39.2	43.8
Solvent atoms	41.0	39.6
Ramachandran plot (%)		
Most favored	90.5	93.6
Additionally allowed	8.7	5.7
Generously allowed	0.8	0.8
Disallowed	0	0
No. of protein atoms	2404	2404
No. of ligand atoms	4	0
No. of solvent atoms	135	57

Values in parentheses are for the highest resolution shell.

$R_w = \Sigma \, || Fo | - | Fc || / \Sigma | Fo |$, $R_{free} = \Sigma \, || Fo | - | Fc || / \Sigma | Fo |$

Chapter 4:

Conclusion and Future Direction

Conclusion and Future direction

In this study, we concentrated on a chimeric Na^+-driven stator (PomA/PotB) and a native Na^+-driven stator (PomA/PomB), respectively, and investigated how the stator gets activated during the step of assembly around rotor. In the case of chimeric stator, PomA/PotBΔL, the R109P mutation and sequential mutations around 109 allow the stator to be in an active state, following massive ions's influx through the mutant stator. The Proline is well known to act as a structural disruptor when it occurs in the middle of α-helices and β-sheets (Moradi *et al.*, 2009). Thus, we speculate that a conformational change caused by the mutation at the α1 helix specific of $MotB_C$ protein brings the flexibility to the periplasmic region of stator, consequently, the mutant stator would work as an active form as wild type stator does. These results emphasize the importance of the α1 helix for the ion translocation and PG layer binding of stator. Furthermore, the results are consistent with the model of H^+-driven stator assembly proposed previously. Until now, there is no structural information of stator in an active form. Thus, to crystallize and resolve the $MotB_C$ with the mutation will afford an evidence for the potential conformational change involved in the α1 helix of $MotB_C$.

With respect to the native Na^+-driven stator, our results indicate that such a large conformational change as suggested in the case of MotBc can not happen in the $PomB_C$. The N-terminal two thirds of α1 (154-164) in $PomB_C$ changes its conformation to be an active state after the channel opening of stator, subsequently the ion influx through the stator complex. In this study, we provide an evidence for structural change involved in the α1 helix and core domain of the B subunit, which is required for the activation of

stator function as well as for anchoring the stator unit. Combining the previous reports (Fukuoka *et al.*, 2009; Kojima *et al.*, 2011), we try to give a clear explanation for working mechanism of native sodium driven stator (Fig. 24). First, the stator diffuses quickly on the membrane (Fig. 24A); when it reaches around rotor, an interaction between rotor and PomA triggers the plug to be open so that sodium ion is attached to Asp24, as a ion binding site (Fig. 24B); simultaneously, the conformational change involved in the C-terminal region of PomB is triggered to maintain channel of the stator to be open, so massive ions are released into inside of cell. It helps the stator anchor to the PG layer and the T ring (Fig. 24C). When the stator does not effectively conduct sodium ions or there is no ion bound to Asp24, the stator perhaps diffuses into membrane pools where many inactive stators exist (Fig. 24D).

Probably other crosslinks (e.g. involved with β1 and α3) regulate the stator function because we noted that the crosslinks between α1 helix and β1 sheet (I164C-V179C; L168C-I177C) do not affect stator function. Some methods in a direct way to detect the conformational change in the $PomB_C$ should be adopted. Furthermore, the mechanism of the dissociation of the stator with the rotor remains to be mysterious (Fig. 24D). One possible approach to resolve this question is to get the structure of full length of the stator at a high resolution to get an insight into the molecular mechanism by which the stator couples sodium ion flow to flagellar rotation.

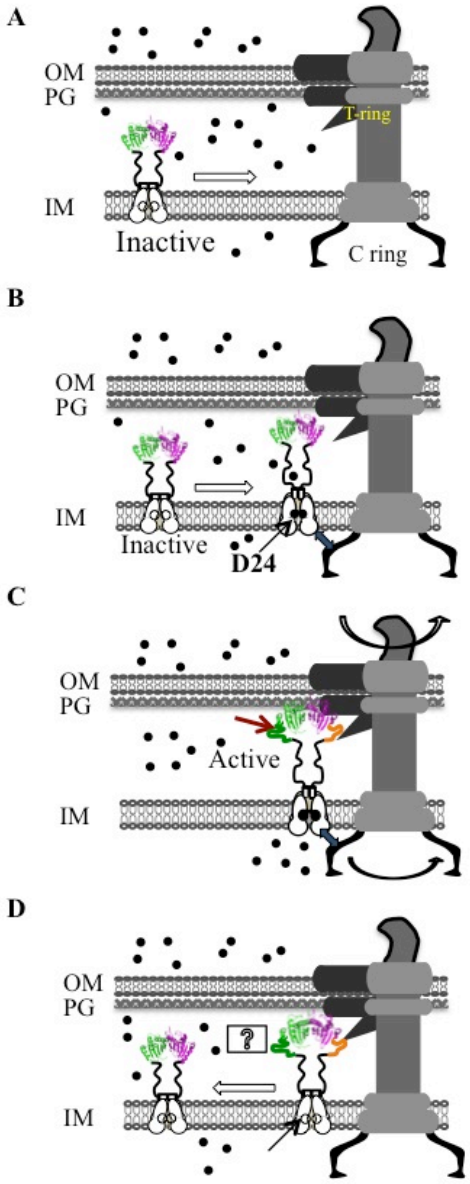

Fig. 24. Working mechanism of native sodium driven stator

(A) First, the stator diffuses quickly on the membrane; (B) When it reaches around rotor, an interaction between rotor and PomA triggers plug to be opened so that sodium ion is attached to Asp24, as ion binding site; (C) Simultaneously, the conformational change involved in the C-terminal region of PomB is triggered to maintain open so that massive ions are released inside of cell and fix stator into the PG layer and T ring; (D) Probably, when stator does not effectively conduct sodium ions or there is no ion at the binding site, it diffuses into membrane pools. Hollow arrow stands for moving direction of the stator. Black arrow stands for ion binding site. Asp24. The arrow in red color means that the helix blow Ile164 is extended in the active state of the stator. Question mark means that the mechanism of disassociation of the stator with the rotor is unknown yet.

Reference

Adams, P. D.*, et al.* (2002). PHENIX: building new software for automated crystallographic structure determination. *Acta crystallographica. Section D, Biological crystallography* 58, 1948-1954.

Aizawa, S.-I. (1996). Flagellar assembly in *Salmonella typhimurium. Mol. Microbiol.* 19, 1-5.

Asai, Y.*, et al.* (1997). Putative channel components for the fast-rotating sodium-driven flagellar motor of a marine bacterium. *J. Bacteriol.* 179, 5104-5110.

Asai, Y., Yakushi, T., Kawagishi, I., and Homma, M. (2003). Ion-coupling determinants of Na^+-driven and H^+-driven flagellar motors. *J. Mol. Biol.* 327, 453-463.

Berg, H. C. (2003). The rotary motor of bacterial flagella. *Annu. Rev. Biochem.* 72, 19-54.

Blake, P. A., Weaver, R. E., and Hollis, D. G. (1980). Diseases of humans (other than cholera) caused by *Vibrios*. *Annu. Rev. Microbiol.* 34, 341-367.

Chen, S.*, et al.* (2011). Structural diversity of bacterial flagellar motors. *The EMBO Journal* 30, 2972-2981.

Chen, X., and Berg, H. C. (2000). Torque-speed relationship of the flagellar rotary motor of *Escherichia coli. Biophys. J.* 78, 1036-1041.

De Mot, R., and Vanderleyden, J. (1994). The C-terminal sequence conservation between OmpA-related outer membrane proteins and MotB suggests a common function in both gram-positive and gram-negative bacteria, possibly in the interaction of these domains with peptidoglycan. *Mol. Microbiol.* 12, 333-334.

Emsley, P., and Cowtan, K. (2004). Coot: model-building tools for molecular graphics. *Acta crystallographica. Section D, Biological crystallography* 60, 2126-2132.

Francis, N. R., Sosinsky, G. E., Thomas, D., and Derosier, D. J. (1994). Isolation, characterization and structure of bacterial flagellar motors containing the switch complex. *J. Mol. Biol.* 235, 1261-1270.

Fukuoka, H.*, et al.* (2009). Sodium-dependent dynamic assembly of membrane complexes in sodium-driven flagellar motors. *Mol. Microbiol.* 71, 825-835.

Guzman, L. M., Belin, D., Carson, M. J., and Beckwith, J. (1995). Tight regulation, modulation, and high-level expression by vectors containing the arabinose

pBAD promoter. *J. Bacteriol.* 177, 4121-4130.

Hizukuri, Y., *et al.* (2009). The peptidoglycan-binding (PGB) domain of the *Escherichia coli* pal protein can also function as the PGB domain in *E. coli* flagellar motor protein MotB. *J. Biochem.* 146, 219-229.

Hosking, E. R., Vogt, C., Bakker, E. P., and Manson, M. D. (2006). The *Escherichia coli* MotAB proton channel unplugged. *J. Mol. Biol.* 364, 921-937.

Johnson, C. N., *et al.* (2012). Ecology of *Vibrio parahaemolyticus* and *Vibrio vulnificus* in the Coastal and Estuarine Waters of Louisiana, Maryland, Mississippi, and Washington (United States). *Appl. Environ. Microb.* 78, 7249-7257.

Kawagishi, I., *et al.* (1996). The sodium-driven polar flagellar motor of marine *Vibrio* as the mechanosensor that regulates lateral flagellar expression. *Mol. Microbiol.* 20, 693-699.

Kawagishi, I., Okunishi, I., Homma, M., and Imae, Y. (1994). Removal of the periplasmic DNase before electroporation enhances efficiency of transformation in the marine bacterium *Vibrio alginolyticus*. *Microbiology.* 140, 2355-2361.

Koebnik, R. (1995). Proposal for a peptidoglycan-associating alpha-helical motif in the C-terminal regions of some bacterial cell-surface proteins. *Mol. Microbiol.* 16, 1269-1270.

Kojima, S., et al. (2008a). Characterization of the periplasmic domain of MotB and implications for its role in the stator assembly of the bacterial flagellar motor. *J. Bacteriol.* 190, 3314-3322.

Kojima, S., et al. (2008b). Insights into the stator assembly of the *Vibrio* flagellar motor from the crystal structure of MotY. *Proc. Natl. Acad. Sci. USA.* 105, 7696-7701.

Kojima, S., et al. (2009). Stator assembly and activation mechanism of the flagellar motor by the periplasmic region of MotB. *Mol. Microbiol.* 73, 710-718.

Kojima, S., et al. (2011). Mutations targeting the C-terminal domain of FliG can disrupt motor assembly in the Na^+-driven flagella of *Vibrio alginolyticus*. *J. Mol. Biol.* 414, 62-74.

Leake, M. C., et al. (2006). Stoichiometry and turnover in single, functioning membrane protein complexes. *Nature* 443, 355-358.

Leslie, A. G. W. (1992). CCP4+ESF-EACMB *Newslett. Protein Crystallogr.* 26, 27-33.

Li, N., Kojima, S., and Homma, M. (2011). Characterization of the periplasmic region of PomB, a Na^+-driven flagellar stator protein in *Vibrio alginolyticus*. *J.*

Bacteriol. 193, 3773-3784.

Macnab, R. M. (2003). How bacteria assemble flagella. *Annual Reviews in Microbiology* 57, 77-100.

Magariyama, Y.*, et al.* (1994). Very fast flagellar rotation *Nature* 371, 752-752.

Mccarter, L., Hilmen, M., and Silverman, M. (1988). Flagellar dynamometer controls swarmer cell differentiation of *V. parahaemolyticus*. *Cell* 54, 345-351.

Mccarter, L. L. (1994a). MotX, the channel component of the sodium-type flagellar motor. *J. Bacteriol.* 176, 5988-5998.

Mccarter, L. L. (1994b). MotY, a component of the sodium-type flagellar motor. *J. Bacteriol.* 176, 4219-4225.

Mccarter, L. L. (2004). Dual flagellar systems enable motility under different circumstances. *J. Mol. Microbiol. Biotechnol.* 7, 18-29.

Moradi, M.*, et al.* (2009). Conformations and free energy landscapes of polyproline peptides. *Proc. Natl. Acad. Sci. USA.* 106, 20746-20751.

Morimoto, Y. V., Che, Y.-S., Minamino, T., and Namba, K. (2010a). Proton-conductivity assay of plugged and unplugged MotA/B proton channel by cytoplasmic pHluorin expressed in *Salmonella*. *Febs. Lett.* 584, 1268-1272.

Morimoto, Y. V.*, et al.* (2010b). Charged residues in the cytoplasmic loop of MotA are required for stator assembly into the bacterial flagellar motor. *Mol. Microbiol.* 78, 1117-1129.

Muramoto, K., and Macnab, R. M. (1998). Deletion analysis of MotA and MotB, components of the force-generating unit in the flagellar motor of *Salmonella*. *Mol. Microbiol.* 29, 1191-1202.

Murphy, G. E., Leadbetter, J. R., and Jensen, G. J. (2006). In situ structure of the complete *Treponema primitia* flagellar motor. *Nature* 442, 1062-1064.

Narita, S.-I.*, et al.* (2013). Protease homolog BepA (YfgC) promotes assembly and degradation of β-barrel membrane proteins in *Escherichia coli*. *Proc. Natl. Acad. Sci. USA.* 110, E3612-3621.

O'neill, J., Xie, M., Hijnen, M., and Roujeinikova, A. (2011). Role of the MotB linker in the assembly and activation of the bacterial flagellar motor. *Acta crystallographica. Section D, Biological crystallography* 67, 1009-1016.

Okabe, M., Yakushi, T., Asai, Y., and Homma, M. (2001). Cloning and characterization of motX, a *Vibrio alginolyticus* sodium-driven flagellar motor gene. *J. Biochem.*

130, 879-884.

Okabe, M., Yakushi, T., and Homma, M. (2005). Interactions of MotX with MotY and with the PomA/PomB sodium ion channel complex of the *Vibrio alginolyticus* polar flagellum. *J. Biol. Chem.* 280, 25659-25664.

Okunishi, I., Kawagishi, I., and Homma, M. (1996). Cloning and characterization of motY, a gene coding for a component of the sodium-driven flagellar motor in *Vibrio alginolyticus*. *J. Bacteriol.* 178, 2409-2415.

Parsons, L. M. L., Lin, F. F., and Orban, J. J. (2006). Peptidoglycan recognition by Pal, an outer membrane lipoprotein. *Biochemistry.* 45, 2122-2128.

Roujeinikova, A. (2008). Crystal structure of the cell wall anchor domain of MotB, a stator component of the bacterial flagellar motor: implications for peptidoglycan recognition. *Proc. Natl. Acad. Sci. USA*. 105, 10348-10353.

Slocum, M. K., and Parkinson, J. S. (1983). Genetics of methyl-accepting chemotaxis proteins in *Escherichia coli*: organization of the tar region. *J. Bacteriol.* 155, 565-577.

Sowa, Y., and Berry, R. M. (2008). Bacterial flagellar motor. *Q. Rev. Biophys.* 41, 103-132.

Sowa, Y*., et al.* (2005). Direct observation of steps in rotation of the bacterial flagellar motor. *Nature* 437, 916-919.

Stolz, B., and Berg, H. C. (1991). Evidence for interactions between MotA and MotB, torque-generating elements of the flagellar motor of *Escherichia coli. J. Bacteriol.* 173, 7033-7037.

Sudo, Y*., et al.* (2009). Comparative study of the ion flux pathway in stator units of proton- and sodium-driven flagellar motors. *Biophysics* 5, 45-52.

Takekawa, N., Li, N., Kojima, S., and Homma, M. (2012). Characterization of PomA mutants defective in the functional assembly of the Na^+-driven flagellar motor in *Vibrio alginolyticus*. *J. Bacteriol.* 194, 1934-1939.

Takekawa, N*., et al.* (2013). Na^+ conductivity of the Na^+-driven flagellar motor complex composed of unplugged wild-type or mutant PomB with PomA. *J. Biochem.* 153, 441-451.

Terashima, H*., et al.* (2006). The *Vibrio* motor proteins, MotX and MotY, are associated with the basal body of Na^+ - driven flagella and required for stator formation. *Mol. Microbiol.* 62, 1170-1180.

Terashima, H., Kojima, S., and Homma, M. (2008). Flagellar motility in bacteria structure and function of flagellar motor. *Int. Rev. Cell. Mol. Biol.* 270, 39-85.

Terashima, H., Kojima, S., and Homma, M. (2010). Functional transfer of an essential aspartate for the ion-binding site in the stator proteins of the bacterial flagellar motor. *J. Mol. Biol.* 397, 689-696.

Terashima, H.*, et al.* (2013). Insight into the assembly mechanism in the supramolecular rings of the sodium-driven *Vibrio* flagellar motor from the structure of FlgT. *Proc. Natl. Acad. Sci. USA.* 110, 6133-6138.

Terauchi, T., Terashima, H., Kojima, S., and Homma, M. (2011). A conserved residue, PomB-F22, in the transmembrane segment of the flagellar stator complex, has a critical role in conducting ions and generating torque. *Microbiology.* 157, 2422-2432.

Thomas, D. R., Francis, N. R., Xu, C., and Derosier, D. J. (2006). The three-dimensional structure of the flagellar rotor from a clockwise-locked mutant of *Salmonella enterica* serovar Typhimurium. *J. Bacteriol.* 188, 7039-7048.

Winn, M. D.*, et al.* (2011). Overview of the CCP4 suite and current developments. *Acta crystallographica. Section D, Biological crystallography* 67, 235-242.

Yakushi, T.*, et al.* (2006). Roles of charged residues of rotor and stator in flagellar rotation: comparative study using H^+-driven and Na^+-driven motors in Escherichia coli. *J. Bacteriol.* 188, 1466-1472.

Yorimitsu, T. (2000). Intermolecular Cross-linking between the Periplasmic Loop3-4 Regions of PomA, a Component of the Na^+-driven Flagellar Motor of *Vibrio alginolyticus*. *J. Biol. Chem.* 275, 31387-31391.

Yorimitsu, T. (2004). Multimeric Structure of the PomA/PomB Channel Complex in the Na^+-Driven Flagellar Motor of *Vibrio alginolyticus*. *J. Biochem.* 135, 43-51.

Yorimitsu, T.*, et al.* (1999). Functional interaction between PomA and PomB, the Na^+-driven flagellar motor components of *Vibrio alginolyticus*. *J. Bacteriol.* 181, 5103-5106.

Zhou, J., Lloyd, S. A., and Blair, D. F. (1998a). Electrostatic interactions between rotor and stator in the bacterial flagellar motor. *Proc. Natl. Acad. Sci. USA.* 95, 6436-6441.

Zhou, J.*, et al.* (1998b). Function of protonatable residues in the flagellar motor of

Escherichia coli: a critical role for Asp 32 of MotB. *J. Bacteriol.* 180, 2729-2735.

Zhu, S., Homma, M., and Kojima, S. (2012). Intragenic Suppressor of a Plug Deletion Nonmotility Mutation in PotB, a Chimeric Stator Protein of Sodium-Driven Flagella. *J. Bacteriol.* 194, 6728-6735.